

AperTO - Archivio Istituzionale Open Access dell'Università di Torino

**Characterization of Cu-exchanged SSZ-13: a comparative FTIR, UV-Vis, and EPR study with Cu-ZSM-5 and Cu- $\beta$  with similar Si/Al and Cu/Al ratios**

**This is the author's manuscript**

*Original Citation:*

*Availability:*

This version is available <http://hdl.handle.net/2318/138531> since 2016-10-08T15:45:58Z

*Published version:*

DOI:10.1039/c3dt50732g

*Terms of use:*

Open Access

Anyone can freely access the full text of works made available as "Open Access". Works made available under a Creative Commons license can be used according to the terms and conditions of said license. Use of all other works requires consent of the right holder (author or publisher) if not exempted from copyright protection by the applicable law.

(Article begins on next page)



# UNIVERSITÀ DEGLI STUDI DI TORINO

*This is an author version of the contribution published on:  
Questa è la versione dell'autore dell'opera:*

**F. Giordanino, P. N. R. Vennestrøm, L. F. Lundegaard,  
F. N. Stappen, S. Mossin, P. Beato, S. Bordiga, C. Lamberti,**

**“Characterization of Cu-exchanged SSZ-13: a comparative  
FTIR, UV-Vis, and EPR study with Cu-ZSM-5 and Cu- $\beta$  with  
similar Si/Al and Cu/Al ratios”,**

*Dalton Trans.*, **42** (2013) 12741-12761.

doi: 10.1039/c3dt50732g

*The definitive version is available at:*

<http://pubs.rsc.org/en/content/articlelanding/2013/dt/c3dt50732g#!divAbstract>

**Published by the Royal Society of Chemistry (RSC)**

# Characterization of Cu-exchanged SSZ-13: a comparative FTIR, UV-Vis, and EPR study with Cu-ZSM-5 and Cu- $\beta$ with similar Si/Al and Cu/Al ratios

Filippo Giordanino,<sup>a</sup> Peter N. R. Vennestrøm,<sup>b,c</sup> Lars F. Lundegaard,<sup>b</sup> Frederick N. Stappen,<sup>d</sup> Susanne Mossin,<sup>d</sup> Pablo Beato,<sup>b</sup> Silvia Bordiga,<sup>a</sup> Carlo Lamberti,<sup>a,\*</sup>

<sup>a</sup> Department of Chemistry, NIS Centre of Excellence and INSTM Reference Center, Via Giuria 7, University of Turin, 10125 Torino, Italy.

<sup>b</sup> Haldor Topsøe A/S, Nymøllevej 55, 2800 Kgs. Lyngby, Denmark

<sup>c</sup> Instituto de Tecnología Química (UPV-CSIC), Universitat Politècnica de Valencia, Consejo Superior de Investigaciones Científicas, Avenida de los Naranjos s/n, 46022 Valencia, Spain

<sup>d</sup> Department of Chemistry, Centre for Catalysis and Sustainable Chemistry, Technical University of Denmark, Kemitorvet 207, 2800 Kgs. Lyngby, Denmark

## Abstract

Cu-SSZ-13 has been characterized by different spectroscopic techniques and compared with Cu-ZSM-5 and Cu- $\beta$  with similar Si/Al and Cu/Al ratios and prepared by the same ion exchange procedure. On *vacuum* activated samples, low temperature FTIR spectroscopy allowed us to appreciate a high concentration of reduced copper centres, *i.e.* isolated Cu<sup>+</sup> ions located in different environments, able to form Cu<sup>+</sup>(N<sub>2</sub>), Cu<sup>+</sup>(CO)<sub>n</sub>(n=1,2,3), and Cu<sup>+</sup>(NO)<sub>n</sub>(n=1,2) upon interaction with N<sub>2</sub>, CO and NO probe molecules, respectively. Low temperature FTIR, DRUV-Vis and EPR analysis on O<sub>2</sub> activated samples revealed the presence of different Cu<sup>2+</sup> species. New data and discussion is devoted to: (i) [Cu–OH]<sup>+</sup> species likely balanced by one framework Al atom; (ii) mono( $\mu$ -oxo)dicopper [Cu<sub>2</sub>( $\mu$ -O)]<sup>2+</sup> dimers observed in Cu-ZSM-5 and Cu- $\beta$ , but not in Cu-SSZ-13. UV-Vis-NIR spectra of O<sub>2</sub> activated samples reveal intense and finely structured d-d quadruplet, unique to Cu-SSZ-13, which is persistent under SCR conditions. This differs from the 22700 cm<sup>-1</sup> band of the mono( $\mu$ -oxo)dicopper species of the O<sub>2</sub> activated Cu-ZSM-5, which disappears under SCR conditions. The EPR signal intensity sets Cu- $\beta$  apart from the others.

**Keywords:** DeNO<sub>x</sub> via NH<sub>3</sub>-SCR, Cu-SSZ-13, *in situ* FTIR, UV-Vis-NIR, EPR

## 1. Introduction

Selective catalytic reduction (SCR) using ammonia as reducing agent is an effective way to remove NO<sub>x</sub> from the exhaust of lean-burn engines.<sup>1</sup> Among the various catalysts tested for this purpose, significant research efforts focused on Cu-exchanged zeolites due to their high activity in lean conditions and their applicability over a wide range of temperatures.<sup>2-4</sup> Over the past two decades significant insight on the mechanism of NO<sub>x</sub> conversion over Cu-zeolites has been obtained and a number of proposals for the structural and chemical nature of the active sites in this reaction have

been made.<sup>5-10</sup> However, a complete picture of the structure-activity relationship for Cu-zeolites in NH<sub>3</sub>-SCR applications is still missing.

Most studies have been carried out on Cu<sup>2+</sup> ion-exchanged Y, ZSM-5 and  $\beta$  zeolites. The main drawback of these medium- and large-pore zeolites was related to the lack of hydrothermal stability at temperatures above 700°C, making them unattractive for commercial applications.<sup>11,12</sup> Recently, Cu-exchanged small-pore zeolites were reported to show high SCR activity even after extensive high-temperature hydrothermal aging.<sup>13-15</sup> Among these zeolites, Cu-SSZ-13 (CHA framework with high Si/Al ratio<sup>16-20</sup>) has received most attention due to its particular high stability.<sup>12</sup> The recent discoveries and the immediate commercial implications of Cu-SSZ-13, have also led to a renewed interest in unraveling the working principle of Cu-zeolites in NH<sub>3</sub>-SCR, as briefly reviewed here below.

Starting from 2010 an increasing number of papers appeared aimed to characterize Cu-SSZ-13 samples and to study its activity in the NH<sub>3</sub>-SCR reaction.<sup>12-14,21-35</sup> In particular, the group of the Pacific Northwest National Laboratory has been one of the most active,<sup>12,13,21-25</sup> reporting first the superior activity of Cu-SSZ-13 with respect of Cu-ZSM-5 and Cu- $\beta$ <sup>13</sup> and then the higher stability of the Cu-SSZ-13 catalyst.<sup>12</sup> In ref. <sup>21</sup> they investigated the effect of Cu loading on the activity. Successively the group started to characterize the catalyst with IR spectroscopy of adsorbed CO and NO,<sup>22,23</sup> with TPR<sup>22,24</sup> and EPR.<sup>24</sup> Finally, they reported a combined DRIFTS-MS studies on the oxidation of adsorbed NH<sub>3</sub> by NO<sub>x</sub> over a Cu-SSZ-13 zeolite.<sup>25</sup> The group of Lobo<sup>27</sup> reported a temperature dependent XRPD investigation on the Cu<sup>2+</sup> location in the framework; of interest is the findings that the CHA framework is more stable to the thermal treatments in its Cu-exchanged form than in its original protonic one. In a successive work,<sup>14</sup> they compared the catalytic activity of Cu-SSZ-13 with that of Cu-SSZ-16, and Cu-SAPO-34 catalyst: the superiority of the catalyst with CHA framework was highlighted. Very active has also been the collaboration between Beale and Weckhuysen group.<sup>28-30</sup> In 2012 they performed an operando, XRPD and Cu K-edge XAFS study.<sup>28</sup> This year, they reported a combined XRPD, solid-state NMR, UV-Vis and Cu- K edge XAFS study on three different samples prepared via different Cu-exchange routes.<sup>29</sup> The group of Ribeiro<sup>31,32</sup> performed an operando Cu-K-edge XAFS study supported by DFT calculations.<sup>31</sup> Ma *et al.*<sup>33</sup> supported the catalytic activity on different Cu-SSZ-13 and Cu-SAPO-34 catalysts with TPR and EPR investigations.

A number of stable Cu species have been postulated to be active sites in SCR reaction, such as dimeric Cu species, isolated cationic species and even CuO<sub>x</sub> nanoclusters.<sup>36</sup> Additionally, the importance of the Cu<sup>2+</sup>/Cu<sup>+</sup> redox chemistry has also been stressed out.<sup>31,37,38</sup>

The Cu speciation in zeolites is influenced by the Cu/Al and the Si/Al ratio,<sup>39-41</sup> which implies that the choice of both ratios during the zeolite synthesis will largely determine the properties of the final material.<sup>42-44</sup> Monovalent cations like alkali metal cations can be easily hosted in the zeolite by coordinating to lattice oxygen adjacent to Al sites.<sup>45,46</sup> In the case of copper, the absence of soluble Cu<sup>+</sup> salts makes the direct insertion of Cu<sup>+</sup> cations in zeolites a non-straightforward task. A high concentration of monovalent Cu<sup>+</sup> sites has been observed only under peculiar exchange conditions, *i.e.* gas<sup>8,47-50</sup> or solid<sup>9,51-55</sup> state phase reaction with CuCl. In such cases the exchange chemistry is relatively clear, leading to a stoichiometric 1:1 H<sup>+</sup>/Cu<sup>+</sup> exchange. It has been shown that Cu<sup>+</sup> cation exchange can also be obtained from a Cu<sup>2+</sup>-exchanged zeolite after a treatment at high temperature *in vacuo* or under inert (usually He) flow.<sup>56-60</sup> However, in this case the situation is less well defined and the chemistry during so called Cu<sup>2+</sup> “self-reduction” is not well understood (*vide infra*).

In principle, classical wet ion-exchange procedure, *i.e.* starting from Cu<sup>2+</sup> salt, should lead to divalent cations like Cu<sup>2+</sup> or oxocations, *e.g.* [Cu–O–Cu]<sup>2+</sup> which can be charge compensated only by a pair of nearby Al sites. From a statistical point of view, Al pairs can be significantly present only in zeolites with a low Si/Al ratio. Theoretical calculations have shown their possible existence in ZSM-5, mordenite, and ferrierite, providing coordination sites for divalent metal oxocations.<sup>61</sup> For high Si/Al ratios charge compensation must follow other ways, and can be achieved by *e.g.* OH<sup>-</sup> groups, resulting in monovalent [Cu–OH]<sup>+</sup> complexes. The mechanism for the above mentioned “self-reduction” of Cu<sup>2+</sup> under *vacuum* or inert flow, is thought to start from the dehydration of two [Cu–OH]<sup>+</sup> ions located close to one framework Al. Two main final products have been suggested: (i) isolated [Cu–O]<sup>+</sup> and Cu<sup>+</sup> species,<sup>62</sup> or (ii) [Cu–O–Cu]<sup>2+</sup> oxocations<sup>63,64</sup> that can condense further under a high temperature treatment to form Cu<sup>+</sup>...Cu<sup>+</sup> pairs.<sup>58,59,65</sup>

A number of different preferred crystallographic sites for Cu<sup>2+</sup> ions have been proposed for the CHA topology. On the bases of XRPD data on Cu-SSZ-13, Fickel *et al.*<sup>27</sup> proposed that Cu<sup>2+</sup> ions are exclusively located on the face of the *d6r* (double six rings) units of the SSZ-13 structure, exhibiting a local coordination very similar to that found in Y zeolite<sup>66</sup> A unique site for Cu<sup>2+</sup> in SSZ-13 zeolite has been also postulated by Korhonen *et al.* On the bases of *ex situ* EXAFS and *in situ* UV-Vis-NIR studies they suggested isolated Cu<sup>2+</sup> slightly shifted towards the edge of the 6-membered rings as active sites for the NH<sub>3</sub>-SCR reaction.<sup>67</sup> On the other hand, a very recent study by Kwak *et al.* suggests that only at low copper content (around Cu/Al = 0.1) Cu predominately occupies the 6-membered ring sites, *i.e.* highly coordinated, stable sites; by increasing the copper content above Cu/Al = 0.3, H<sub>2</sub>-TPR and FT-IR evidenced the presence of another more accessible copper site likely located inside the large cages of the CHA topology.<sup>22</sup> From a Cu<sup>+</sup> luminescence study, the presence of two different copper sites in reduced Cu<sup>2+</sup>-CHA has also been proposed by

Dedecek *et al.*<sup>68</sup> These conclusions have been recently supported on Cu-SSZ-13 by the group of Kwak<sup>23,24</sup> Furthermore two authoritative reviews have recently appeared by Venelderen *et al.*<sup>69</sup> and Deka *et al.*<sup>30</sup>, where the location of copper cations in zeolites were widely discussed.

Despite the abundance of recent research studies on Cu-SSZ-13, two main questions seem to be still open in the literature, and are investigated in this study: the first one refers to the location of copper in the SSZ-13 framework; the second question refers to the formation of oxo-dimers in Cu-SSZ-13, *e.g.* [Cu–O–Cu]<sup>2+</sup>.

From what has been discussed so far, it becomes evident that the possibility to investigate the effect of the zeolite topology on the copper sitting can be meaningful only if comparison is made on a set of samples with similar Si/Al and Cu/Al ratios. Moreover, the Si/Al ratio has to be sufficiently low, (*i.e.* < 30), and the Cu/Al sufficiently high, (*i.e.* > 0.3) to allow [Cu–O–Cu]<sup>2+</sup> oxocations to be formed in a significant amount.<sup>70</sup> For this reason SSZ-13 has been synthesized *ad hoc* with a Si/Al ratio of 13, in order to be comparable with commercial ZSM-5 and  $\beta$  zeolites characterized by Si/Al = 11 and 13, respectively. Care has been taken in order to reach a comparable cationic exchange level in the three samples; thus samples were synthesized with Cu/Al ratios of 0.44, 0.42 and 0.44 for SSZ-13, ZSM-5 and  $\beta$ , respectively. The results of the elemental analysis are reported in Table 1.

**Table 1** Elemental analysis of the samples obtained with the ICP- OES technique, and reported in atomic ratios.

ICP- OES		
Sample	Si/Al	Cu/Al
Cu-ZSM-5	10.5	0.423
Cu-SSZ-13	13.1	0.444
Cu- $\beta$	13.0	0.437

On this set of comparable samples, the local cation environment and geometry was investigated by low temperature IR spectroscopy of adsorbed N<sub>2</sub>, CO and NO probe molecules, DRUV-Vis-NIR and EPR spectroscopies. As it will be shown in the present work the *vacuum* treatment leads to almost exclusively Cu<sup>+</sup>, whereas an oxidative O<sub>2</sub> treatment allow us to maintain and investigate predominately Cu<sup>2+</sup> species. Since activation treatment is decisive, both *vacuum* and O<sub>2</sub> activation procedueres have been considered.

## 2. IR spectroscopy

IR spectroscopy of adsorbed probe molecules is a powerful technique in the characterization of surface sites of both porous and non-porous high surface area materials.<sup>71-76</sup> The choice of probe molecule is a crucial point in this approach; different probe molecules may be able to reveal

different aspects of the investigated surface, and often the combined use of markedly different probes is the key to reach a comprehensive understanding of the surface.<sup>75</sup> In the present study we used N<sub>2</sub>, CO and NO probes to characterize Cu-exchanged SSZ-13, ZSM-5  $\beta$  and zeolites. The use of a weakly interacting probe as N<sub>2</sub> allows to minimize the perturbation induced by the probe and so to better discriminate among similar adsorption sites. The use of CO allows selectively towards Cu<sup>+</sup> sites, while NO can probe both Cu<sup>+</sup> and Cu<sup>2+</sup> sites. In all cases probe adsorption has been performed at low or even liquid nitrogen temperature to also detect the surface sites characterized by a weak interaction with the probe (not visible in RT experiments). Note that for NO low temperature experiments are essential because NO is reactive at RT and therefore does not act solely as a probe.<sup>8</sup>

## 2.1. IR spectroscopy of adsorbed N<sub>2</sub>

### 2.1.1. Interaction of N<sub>2</sub> with Cu<sup>+</sup> sites

N<sub>2</sub> molecule interacts with cuprous ions inside zeolites gives a  $\nu(\text{NN})$  band in the 2300-2290 cm<sup>-1</sup> region,<sup>8,77</sup> *i.e.* significantly downward shifted, with respect to the (Raman active) gas-phase value of 2321 cm<sup>-1</sup>. The bathochromic shift could be explained in terms of chemical interaction involving molecular orbitals (MO) of the probe molecule and suitable d orbital of the metal cation.<sup>75</sup> For dinitrogen, the corresponding MOs are 3 $\sigma_g$  which acts as an electron donor, and the empty 1 $\pi_g$  which is the electron acceptor. Both the  $\sigma$ -donor and the  $\pi$ -acceptor interactions weaken the N $\equiv$ N bond, thus explaining the observed bathochromic shift in the Cu<sup>+</sup>(N<sub>2</sub>) adducts.<sup>72</sup> Interaction of N<sub>2</sub> with Cu<sup>2+</sup> and with H<sup>+</sup> is much weaker,<sup>78</sup> consequently we investigate here only the interaction on the *vacuum* activated zeolites (Fig. 1) with the aim to differentiate the Cu<sup>+</sup> sites generated during the *vacuum* treatment due to “self-reduction”.

The IR spectra of N<sub>2</sub> adsorbed on *vacuum* activated Cu-SSZ-13 is reported in Fig. 1. A predominant band, centered at 2293 cm<sup>-1</sup>, is observed starting from low coverages. This component increases in intensity upon increasing coverage without shifting, while a second component centered around 2300 cm<sup>-1</sup>, progressively develops. Both components are assigned to Cu<sup>+</sup>(N<sub>2</sub>) stable complexes.<sup>8,77</sup> The presence of two components in the spectrum of Cu-SSZ-13 implies the presence of two significantly different (in terms of the cation local environment) Cu<sup>+</sup> sites, supporting the conclusions raised by Dedecek *et al.*<sup>68</sup> and by the group of Richland.<sup>23,24</sup> Involved Cu<sup>+</sup> sites behaves as isolated adsorbing sites for N<sub>2</sub>, because of the invariance of the corresponding IR band upon pressure changes.

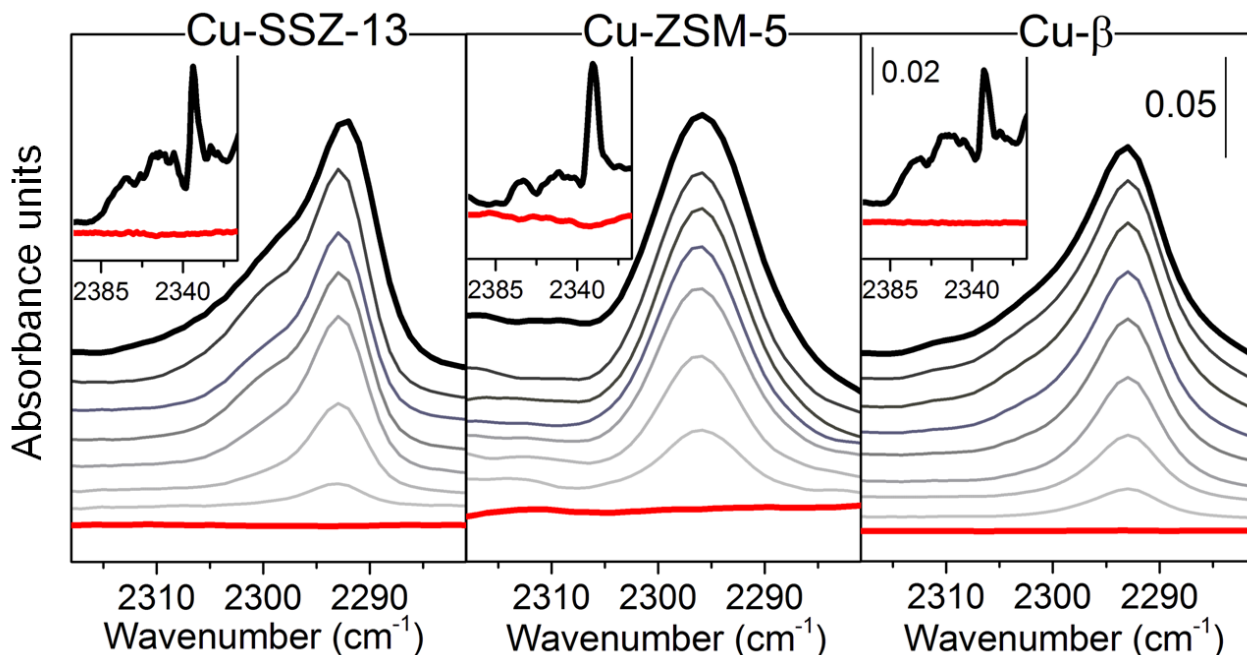


**Fig. 1** Low temperature ( $\sim 100$  K) IR spectra of  $N_2$  dosed at increasing equilibrium pressure (from  $10^{-2}$  to 5 Torr) on *vacuum* activated Cu-zeolites. Red curves show background spectra (*i.e.* before  $N_2$  dosage), black curves refer to highest  $N_2$  coverage, while fading curves refer to intermediate adsorption steps.

A single and symmetric band centered at  $2296\text{ cm}^{-1}$  is observed on *vacuum* activated Cu-ZSM-5 (Fig. 1). Also in this case the frequency of the band is coverage independent. This frequency is almost equivalent to that found on a  $Cu^+$ -ZSM-5 prepared by gas phase exchange with  $CuCl$ ,<sup>8</sup> see also Table 2. This implies that, if present, different  $Cu^+$  cationic sites in ZSM-5 are characterized by a very similar local environment that cannot be discriminated by  $N_2$  adsorption. The spectra of  $N_2$  adsorbed on Cu- $\beta$  (Fig. 1) are dominated by a coverage independent component at  $2293\text{ cm}^{-1}$ . A second component, less intense and resolved than in the Cu-SSZ-13 case, develops at the higher coverages around  $2300\text{ cm}^{-1}$ .

**Table 2**  $\tilde{\nu}(NN)$ , stretching frequencies of dinitrogen adducts formed on  $Cu^+$  sites in Cu-exchanged zeolites and zeotypes, and on supported  $Cu_2O$ . sh = shoulder.

Sample	$\tilde{\nu}(NN)$ ( $\text{cm}^{-1}$ )	Reference
Cu-SSZ-13	2293, 2300 (sh)	this study
Cu-ZSM-5	2296	this study
Cu- $\beta$	2293, 2300 (sh)	this study
Na-Cu-ETS-10(A) $Cu^+$ site	2281	79
Na-Cu-ETS-10(B) $Cu^+$ site	2285	79
Cu-MOR	2299	77
Cu-ZSM-5	2295	8
$Cu_2O/SiO_2$	2283	79

The fact that the bathochromic shift of the main component is larger in Cu-SSZ-13 and Cu- $\beta$  than in Cu-ZSM-5 implies that the dominant  $Cu^+$  sites in SSZ-13 and  $\beta$  are able to perform a more efficient  $\sigma$ -donation and  $\pi$ -back-donation process with the MO of the  $N_2$  molecule. This could be associated



to a larger space in the cation vicinity, and or to a more effective iconicity of the cation in case of Cu-SSZ-13 and Cu- $\beta$ .

In both Cu-SSZ-13 and Cu- $\beta$  samples, the less abundant Cu<sup>+</sup> sites, responsible of the shoulder around 2300 cm<sup>-1</sup>, interacts with N<sub>2</sub> in a similar way that the Cu<sup>+</sup> cations hosted in the MOR framework,<sup>77</sup> see Table 2. The absence of any adsorption around 2283 cm<sup>-1</sup> testifies that no undesired Cu<sub>2</sub>O extra-phase<sup>79</sup> is present in the three samples.

### 2.1.2. Interaction of N<sub>2</sub> with Brønsted sites and Al<sup>3+</sup> extra-framework sites

Bands at frequencies higher than 2324 cm<sup>-1</sup> (Raman band of N<sub>2</sub> physisorbed in 4A molecular sieve)<sup>80</sup> reveal the presence of polarizing adsorption sites, interacting with N<sub>2</sub> by mean of Coulomb force only.<sup>78,81</sup> The insets in Fig. 1 show this region, that is characterized in all cases by a sharp band at 2334-2332 cm<sup>-1</sup> and a complex broad absorption with at least two maxima in the 2280–2240 cm<sup>-1</sup> region. In particular N<sub>2</sub> adsorbed on Brønsted sites is observed at 2334, 2332 and 2332 cm<sup>-1</sup> in the Cu-SSZ-13, Cu-ZSM-5 and Cu- $\beta$  frameworks, respectively. The higher upward shift of  $\nu(\text{NN})$  observed in Cu-SSZ-13 reflects a slightly higher acidity of this zeolite with respect to Cu-ZSM-5 and Cu- $\beta$  ones. This fact is also confirmed by the slightly higher bathochromic shift, undergone by the  $\nu(\text{OH})$  band in Cu-SSZ-13 upon interaction with N<sub>2</sub>, see Table 3. Such a small difference in the acidity strength is hardly detected by a probe molecule that acts as a very weak Lewis base as N<sub>2</sub> (proton affinity = 418 kJ mol<sup>-1</sup>); the use of a relatively stronger base as CO (proton affinity = 594 kJ mol<sup>-1</sup>, vide infra Section 2.2.2) will allow a much better discrimination among different Brønsted sites.

**Table 3** Frequency of Brønsted sites hosted in Cu-SSZ-13, Cu-ZSM-5 and Cu- $\beta$  zeolites (column 3) and spectroscopic determination of their acidity strength (columns 5-7), as revealed by the bathochromic shift of the  $\nu(\text{OH})$  mode upon interaction with N<sub>2</sub> and CO probes and by the hypsochromic shift of  $\nu(\text{NN})$  and  $\nu(\text{CO})$  modes. Values are obtained from the spectra reported in Fig. 1 (insets), Fig. 2, Fig. 3 and Fig. 4. The spectra in the  $\nu(\text{OH})$  region corresponding to the experiments reported in Fig. 1 were not reported for sake of brevity. All frequencies and related shifts are reported in cm<sup>-1</sup>.

activation	zeolite framework	unperturbed $\tilde{\nu}(\text{OH})$ Brønsted acid sites	N <sub>2</sub> adsorption		CO adsorption	
			$\Delta\tilde{\nu}(\text{OH})$	$\Delta\tilde{\nu}(\text{NN})$	$\Delta\tilde{\nu}(\text{OH})$	$\Delta\tilde{\nu}(\text{CO})$
<i>vacuum</i>	Cu-SSZ-13	3612, 3595	-118, -99	+10	-336, -319	+30
<i>vacuum</i>	Cu-ZSM-5	3613	-117	+8	-300	+27
<i>vacuum</i>	Cu- $\beta$	3610	-116	+8	-288	+27
O <sub>2</sub>	Cu-SSZ-13	3612, 3595	-	-	-325, -308	+31
O <sub>2</sub>	Cu-ZSM-5	3613	-	-	-312	+30
O <sub>2</sub>	Cu- $\beta$	3610	-	-	-301	+30

Conversely, N<sub>2</sub> is more suited than CO in the detection of a very small fraction of strong Lewis sites such as extra-framework Al<sup>3+</sup> species<sup>78,81</sup> thanks to the dramatic increase of the absorption coefficient of the  $\nu(\text{NN})$  mode when the molecule is adsorbed on an high polarizing Lewis center,

able to cause a stronger induced dipole on the molecule that, in the gas phase is IR inactive. These observations confirm the presence of small amounts of extra-framework  $\text{Al}^{3+}$  in all materials, which could be formed during the *vacuum* treatment or already present in the material before the treatment.

## 2.2. IR spectroscopy of adsorbed CO: interaction with $\text{Cu}^+$ and Hydroxyl groups

It is widely established by IR that as a weak base CO molecules interact with coordinatively unsaturated cations, *i.e.* Lewis sites, including those hosted in zeolites.<sup>72,73,75,76</sup> The high coordinative unsaturation of  $\text{Cu}^+$  cations hosted in zeolites is further demonstrated by their ability to form, depending on partial pressure of CO and temperature, carbonyl complexes, *i.e.*  $\text{Cu}^+(\text{CO})_n$  ( $n = 1,2,3$ ).<sup>8,47,66,82-86</sup> Conversely, due to the weaker interaction between  $\text{Cu}^{2+}$  and CO the corresponding  $\text{Cu}^{2+}(\text{CO})$  complexes are very unstable and difficult to detect even at low temperature,<sup>71,87</sup> particularly when they are in co-presence with  $\text{Cu}^+$  sites. This last reason explains why CO molecules are commonly employed to probe only  $\text{Cu}^+$  sites. In addition to Lewis metal centre acidity, residual acidity due to hydroxyl groups in the zeolite (*e.g.* strong Brønsted and silanols groups) is commonly present, especially in those samples where the Cu/Al ratio is far away from the stoichiometric exchange level (Cu/Al = 0.5); contextually adsorbed CO can be employed to probe the electrostatic fields generated by these species.<sup>45,46,72,88</sup> Therefore, a detailed overview of all the acidic species is required and spectra analysis of adsorbed CO needs to be performed on both  $\nu(\text{OH})$  and  $\nu(\text{CO})$  regions. Due to the complexity of the data, the results discussion is divided in sub-sections.

### 2.2.1. Effects of low-medium CO coverage in Cu-SSZ-13: $\nu(\text{OH})$ and $\nu(\text{CO})$ regions

The IR spectra of CO adsorbed on Cu-SSZ-13 are shown in Fig. 2. Upper and lower parts of the figure correspond to *vacuum* and  $\text{O}_2$  activated zeolite, respectively. As mentioned above, spectra are reported in both  $\nu(\text{OH})$  region (parts a and c) and  $\nu(\text{CO})$  region (parts b and d). Activated samples (red curves, parts a and c) show complex absorption bands in the region  $3800\text{-}3000\text{ cm}^{-1}$ , typical of OH groups located in different environment of the zeolite matrix. More specifically, at higher frequencies a maximum around  $3740\text{ cm}^{-1}$  representing (OH) modes of virtually isolated silanol groups located on the external surface of the zeolite is observed. The less intensive bands in the range  $3720\text{-}3620\text{ cm}^{-1}$  are related to the internal silanols in different environments.<sup>89,90</sup> At lower frequencies the typical band related to strong acidic Brønsted sites appears around  $3610\text{ cm}^{-1}$ .<sup>18</sup> In particular two additional tails occur: (i) the feature at  $3597\text{ cm}^{-1}$  has been observed in the parent material H-SSZ-13, and it has been associated to the protons not directly exposed to the eight-

membered ring window of the CHA cage;<sup>18,19</sup> (ii) another broad tail occurs at lowest frequencies ( $3500\text{ cm}^{-1}$ ) which suggests the presence of silanol groups interacting through medium/strong H-bonds in so-called silanol nests (*i.e.*, structural defects). Additionally, in the spectrum of  $\text{O}_2$  activated Cu-SSZ-13 (red curve of Fig. 2c) a new band at  $3657\text{ cm}^{-1}$  is clearly observed (marked by the asterisk). The origin and the nature of this band (not observed on *vacuum* activated sample) are discussed in more detail in Section 2.2.3.

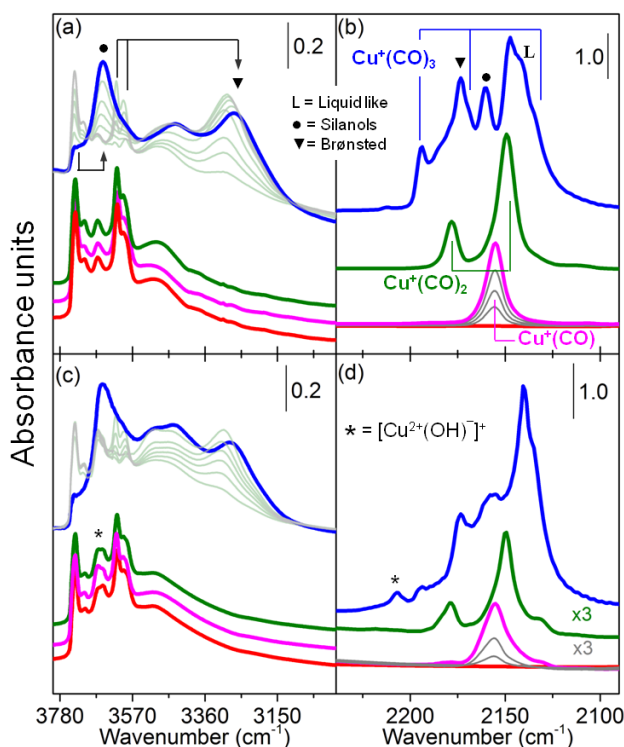


**Fig. 2** Low temperature ( $\sim 100\text{ K}$ ) IR spectra of CO dosed on Cu-SSZ-13. Upper parts (a) and (b) refers to *vacuum* activated zeolite, while lower parts (c) and (d) refers to  $\text{O}_2$  activated zeolite. Parts (a) and (c):  $\nu(\text{OH})$  region ( $3800 - 3000\text{ cm}^{-1}$ ). Parts (b) and (d):  $\nu(\text{CO})$  region ( $2270 - 2080\text{ cm}^{-1}$ ). Red curves show background spectra (*i.e.* before CO dosage); magenta and green curves refer to low and intermediate  $P_{\text{CO}}$ , respectively, approximately corresponding to the saturation of mono- and di-carbonyl complexes. Dark gray curves refer to intermediate absorption steps before reaching the saturation of monocarbonyl complexes. Light gray curves refer to intermediate coverages between dicarbonyl complexes saturation and the highest  $P_{\text{CO}}$  (blue curve).

At low CO coverage (parts b and d, dark grey and magenta spectra) the typical band at  $2155\text{ cm}^{-1}$  due to monocarbonyl  $\text{Cu}^+(\text{CO})$  complexes is observed. The band is significantly more intense in case of *vacuum* activated sample, confirming the higher concentration of  $\text{Cu}^+$  ions in comparison with the  $\text{O}_2$  activated sample. The position of the observed C–O stretching in  $\text{Cu}^+$  monocarbonyls (to be compared with vibration of gaseous CO,  $2143\text{ cm}^{-1}$ ) is the compromise between three effects:<sup>49,75,91,92</sup> (i) blue shift due to the electrostatic interaction with the cation centre (Stark effect); (ii) blue shift due to  $\sigma$ -coordination ( $\text{Cu}^+ \leftarrow \text{CO}$ ) between the filled CO  $5\sigma$  orbital (C-end lone pair) and empty orbital of suitable energy of copper ion (acting as Lewis acidic centre); (iii) red shift due to  $\pi$  back-donation ( $\text{Cu}^+ \rightarrow \text{CO}$ ) of electrons from partially filled d orbital of  $\text{Cu}^+$  to  $\pi^*$  antibonding orbitals of CO. In this case, contributions (i) and (ii) are predominant, resulting in  $\Delta\tilde{\nu}(\text{CO}) > 0$ . As

a global result of the synergic effect between the three bonding contributions, the corresponding complexes are highly stable persisting even after long evacuation time at room temperature (thus  $-\Delta H_{\text{ads}}$  is in the 90-120 kJ mol<sup>-1</sup> range).<sup>49,75,93-96</sup>

By increasing the CO pressure two distinct bands at 2178 and 2148 cm<sup>-1</sup> grow proportionally (parts b and d, green spectra). These two bands have been observed in other Cu<sup>+</sup>-zeolites and they are associated to the symmetric and asymmetric stretching modes of the Cu<sup>+</sup>(CO)<sub>2</sub> complexes, respectively.<sup>8,47,66,82-86,97</sup> Cu<sup>+</sup> sites formed in Cu-SSZ-13 zeolite upon *vacuum* and oxidative treatments are able to form Cu<sup>+</sup>(CO) and Cu<sup>+</sup>(CO)<sub>2</sub> complexes having exactly the same  $\nu(\text{CO})$  stretching frequencies, with the only differences that those formed in presence of O<sub>2</sub> are much less abundant (by a factor 4) and are more inhomogeneous: the FWHM of the monocarbonyl band is 9 and 14 cm<sup>-1</sup>, respectively. In both cases these bands are still quite sharp and symmetric suggesting the presence of only one Cu<sup>+</sup> site. This observation implies that CO is not able to discriminate the two different Cu<sup>+</sup> sites observed using N<sub>2</sub> as probe (see Fig. 1). This apparent contradiction is explained by the strong interaction between CO and Cu<sup>+</sup> that is able to modify the original position of Cu<sup>+</sup> (solvation effect):<sup>47,66,98</sup> in other words, two Cu<sup>+</sup> sites having a different sitting may form very similar carbonyl complexes.<sup>66</sup>

The interpretation of the IR spectra corresponding to the medium-low CO coverages discussed so far was simple because the fact that the  $-\Delta H_{\text{ads}}$  of both mono- and di-carbonyl complexes is much higher than that of CO adsorbed on OH groups implies that: (i) CO adsorption does not affect the OH population of the zeolite, and (ii) cuprous carbonyls are the only species observed in the  $\nu(\text{CO})$  stretching region. Indeed corresponding spectra reported in parts (a) and (c) of Fig. 2 (magenta and green curves) are definitely not perturbed compared to the activated sample (red curve) and no contributions of OH $\cdots$ CO adducts in the  $\nu(\text{CO})$  are clearly observed.

Finally, on both *vacuum* and O<sub>2</sub> activated samples, a minimal amount of coordinatively unsaturated Al<sup>3+</sup> extra-framework species is detected. Al<sup>3+</sup> $\cdots$ CO adducts results in a complex and broad band in the 2235-2220 cm<sup>-1</sup> region<sup>46,99,100</sup> (not reported in the interval shown in Fig. 2b,d and having a maximum intensity as low as  $2 \times 10^{-2}$  a.u.; see Fig. S1 in ESI), that starts to be populated once the Cu<sup>+</sup>(CO)<sub>2</sub> complexes are saturated and before the formation of OH $\cdots$ CO adducts. On this band, we disagree with Szanyi *et al.*<sup>23</sup> who attributed a Cu<sup>2+</sup>(CO) complex to the band at 2220 cm<sup>-1</sup> observed on Cu-SSZ-13 sample after CO reduction at 573 K and subsequently *vacuum* activated at 773 K.

### 2.2.2. Effects of high CO coverage in Cu-SSZ-13: $\nu(\text{OH})$ and $\nu(\text{CO})$ regions

At higher CO coverage the spectra become more complex because the low  $-\Delta H_{\text{ads}}$  value<sup>96</sup> of tricarbonyls, makes the addition of a third CO molecule to Cu<sup>+</sup>(CO)<sub>2</sub> complexes concomitant with

the formation of adducts on Brønsted sites and on the external silanols, resulting in an overlapping of bands in the  $\nu(\text{CO})$  stretching region (blue curves in Fig. 2b,d). The interaction of CO with residual OH groups is observed in the  $\nu(\text{OH})$  stretching region starting from the light grey curves referring to intermediate adsorption steps before reaching the maximum coverage (blue curves). In particular, increasing CO coverage leads to a gradual erosion of Brønsted sites bands (3610 and 3597  $\text{cm}^{-1}$  bands) with the parallel appearance of a component around 3300  $\text{cm}^{-1}$  due to  $\nu(\text{OH})$  of  $\text{OH}\cdots\text{CO}$  adducts. In SSZ-13 system, the presence of a single red-shifted component suggests that the acidity of the two families of Brønsted sites, measured by CO, is comparable. Looking to the quantitative values of the red shifts (Table 1) we observe a decreased acid strength of the Brønsted sites in the  $\text{O}_2$  activated sample where  $\Delta\tilde{\nu}(\text{OH}) = -325 \text{ cm}^{-1}$  while a value of  $-336 \text{ cm}^{-1}$  is observed for the *vacuum* activated sample. This modulation suggests that Brønsted acidic strength is influenced by the pretreatment and/or oxidation state of copper in the zeolite system, which could be relevant for the SCR mechanism, as the importance of redox behavior between  $\text{Cu}^{2+}$  and  $\text{Cu}^+$  has been stressed out earlier.<sup>31,37,38</sup> Furthermore the modulation in acidity could also play a relevant role as the Brønsted acid sites acts as a sink for ammonia in the reaction without their direct participation.<sup>4</sup>

Higher CO pressures also lead to interaction between CO and silanol groups<sup>18</sup> as testified by the erosion of the bands at around 3740  $\text{cm}^{-1}$  and a parallel growth around 3650  $\text{cm}^{-1}$ . In the  $\nu(\text{CO})$  stretching region CO adsorbed on Brønsted and silanols sites results in components at 2173 and 2160  $\text{cm}^{-1}$ , respectively<sup>100,101</sup> (see triangle and circle symbols in Fig. 2b), while at the highest coverages the band at 2138  $\text{cm}^{-1}$  due to liquid-like CO physisorbed in the zeolite channels<sup>100,102,103</sup> becomes the dominant feature (blue spectrum in Fig. 2b,d).

The analysis of  $\nu(\text{CO})$  signals due to CO adducts on OH groups is simpler on the  $\text{O}_2$  activated sample as compared to *vacuum* activated sample as a consequence of the smaller amount of  $\text{Cu}^+$  leading to less signal from  $\text{Cu}^+(\text{CO})_n$  complexes.

Surprisingly the intensity of the Brønsted groups is not enhanced in the *vacuum* activated sample compared with the  $\text{O}_2$  activated one (compared red curves in Fig. 2a and c, respectively) meaning that the so called “self-reduction” of  $\text{Cu}^{2+}$  into  $\text{Cu}^+$  during the *vacuum* activation process is not generating new protonic  $\text{H}^+$  sites to compensate the loss of one positive charge for all copper atoms. This observation has deep implications, because it rules out the presence of a significant fraction of  $\text{Cu}^{2+}$  able to balance the negative framework charge induced by two adjacent Al atoms and implies that most of the cupric sites are inserted in form of monovalent complexes such as  $[\text{Cu}-\text{OH}]^+$  (*vide infra* Section 2.2.3).

Notwithstanding the complexity of the high coverage spectrum, based on the IR experiments performed on zeolites exchanges with CuCl from the gas phase,<sup>8,47,82,84</sup> where only bands due to cuprous carbonyls are observed in the  $\nu(\text{CO})$  stretching region, it is possible to assign the three components of the  $\text{Cu}^+(\text{CO})_3$  complexes to the bands at 2194, 2169, and 2134  $\text{cm}^{-1}$ , the last two being just shoulders. The significant presence of the doublet of the  $\text{Cu}^+(\text{CO})_2$  complexes in the highest coverage spectrum implies that only a minor fraction of  $\text{Cu}^+$  sites is able to coordinate a third CO molecule. This fraction is again lower in the  $\text{O}_2$  activated sample than in the *vacuum* activated one.

### 2.2.3. Interaction of CO with dehydrated $[\text{Cu}-\text{OH}]^+$ sites in Cu-SSZ-13

The quite sharp ( $\text{FWHM} < 6 \text{ cm}^{-1}$ ) band at 2207  $\text{cm}^{-1}$  appearing at the highest CO coverages, only present in the  $\text{O}_2$  activated sample, has a different origin. Following intermediate CO coverages between the green and the blue spectra (not shown in Fig. 2d, see Fig.S1 in ESI) the 2207  $\text{cm}^{-1}$  band develops when the  $\text{Al}^{3+}\cdots\text{CO}$  adducts are almost saturated. It is interesting to note that the appearance of the 2207  $\text{cm}^{-1}$ -band in the  $\nu(\text{CO})$  stretching region is accompanied by the presence of a new band in the  $\nu(\text{OH})$  stretching region at 3657  $\text{cm}^{-1}$ , and that the growth of the former is correlated to the erosion of the latter (see light grey spectra in Fig. 2c). Consequently, this new band could be tentatively attributed to  $[\text{Cu}-\text{OH}]^+$  species formed upon dehydration.

### 2.2.4. Attribution of the weak band around 2135 $\text{cm}^{-1}$ in Cu-SSZ-13

At low to medium CO coverages (*i.e.* up to the green curves in Fig. 2b,d) another shoulder is observed at around 2134  $\text{cm}^{-1}$  in addition to the  $\text{Cu}^+$  mono- and di-carbonyl bands. The presence of this band is furthermore visually more evident in the case of the  $\text{O}_2$  activated sample because of the lower intensities from copper-carbonyl bands. This is the region where the  $\nu(\text{CO})$  is observed for CO adsorbed on the  $\text{Cu}_2\text{O}$  phase,<sup>104</sup> and several studies confirmed the presence of a nanostructured  $\text{Cu}_2\text{O}$  extra-phase in zeolites over-exchanged with copper<sup>79,105-107</sup> generated during the high temperature treatment. In the present case, we can rule out this kind of assignment because we do not see the typical IR bands due to mono- and di-nitrosyl adducts formed on  $\text{Cu}_2\text{O}$  upon NO adsorption (*vide infra* Fig. 5a in Section 2.3). Moreover, UV-Vis spectra (*vide infra* Section 2.2) do not see the strong energy gap at 16300  $\text{cm}^{-1}$  of  $\text{Cu}_2\text{O}$ .<sup>79</sup>

The existence of CO adsorption complexes on heterogeneous dual cationic sites, where the CO molecule interacts simultaneously with copper and alkali metal cations via C- and O- end, respectively, has been evidenced by absorption bands at 2138 and 2112  $\text{cm}^{-1}$  in Cu-M-FER zeolites (M = K, Cs).<sup>108</sup> In the same work, CO adsorption complexes on dual cation sites were not observed

in Cu,H-FER and Cu-Na-FER zeolites,<sup>108</sup> making hard to associate the 2134 cm<sup>-1</sup> band to a dual cation adsorption centre in Cu-SSZ-13; indeed M can be only H or Cu in our case, and Cu has the same ionic radius than Na.<sup>49</sup>

Recently Szanyi *at al.* have assigned a similar band at 2135 cm<sup>-1</sup> to CO molecule adsorbed onto Cu<sup>+</sup> ions located in constrained environments of SSZ-13 structure (*i.e.* in six-membered rings). This conclusion is also supported by the observation that Cu<sup>+</sup> di-carbonyl species were only observed for Cu<sup>+</sup> ions located in the large cavities and channels of these zeolites, but not on cations sitting in more constrained framework sites.<sup>23</sup> Our results strictly support this last assignment.

### 2.2.5 Comparison with the experiments performed on Cu-ZSM-5 and Cu-β

As the Cu-SSZ-13 case (Fig. 2) has been treated in extensive detail, FTIR experiments of CO adsorption on Cu-ZSM-5 (Fig. 3) and Cu-β (Fig. 4) will only be briefly commented.

Bands shape of both Cu<sup>+</sup>(CO) and Cu<sup>+</sup>(CO)<sub>2</sub> complexes are tailed in the low frequency side, suggesting heterogeneity of Cu<sup>+</sup> location in ZSM-5 and the presence of two distinguishable family of sites for Cu-β. Note that this was not the case for the Cu-ZSM-5<sup>8,98</sup> and Cu-β<sup>85</sup> materials prepared with stoichiometric gas phase reaction with CuCl. In those cases, low Al loading associated to a different exchange procedure imply that Cu species locate in position not equivalent to those where Cu<sup>2+</sup> species are exchanged in the materials here investigated.

*Vacuum* and O<sub>2</sub> activation treatments generate Cu<sup>+</sup> sites able to form mono-, di- and tri-carbonyls characterized by exactly the same ν(CO) stretching frequencies. These frequencies change only by few cm<sup>-1</sup> from one topology to the others, see Table 4. This is a very general observation that can be extended to other frameworks as well as to other Cu-exchange procedures. For the three frameworks investigated here, and in particular in case of Cu-ZSM-5, Cu<sup>+</sup> sites are much less prone to form tri-carbonyls adducts in the O<sub>2</sub> activated sample. Moreover, for all three frameworks the acidity strength of the Brønsted sites (in the order Cu-SSZ-13 > Cu-ZSM-5 ≈ Cu-β in *vacuum* activated samples) is significantly affected by the oxidative procedure. In particular Cu-ZSM-5 and Cu-β show an increased Δν̄ (OH), while Cu-SSZ-13 reveals a slightly decrease of Δν̄ (OH) (see Table 3). The concentration of Brønsted sites (estimated from the corresponding band intensity) is not strongly affected by the activation treatment. This observation supports the idea that the charge balance is not made by bare Cu<sup>2+</sup> species. In Cu-ZSM-5 external silanols are much less abundant (silanols band less pronounced, indicating larger crystals size for the used in this study). In both the ν(OH) and ν(CO) stretching regions, bands associated to dehydrated [Cu–OH]<sup>+</sup> species are well observed for Cu-ZSM-5, but only to a small extent in Cu-β. Moreover the abundance of these species is also associated with the amount of Al loading that affect Al distribution (*i.e.* Al pairs).

The broad component in the high frequency region of the blue spectrum in Fig. 5d is centered at 2220  $\text{cm}^{-1}$  and is ascribable to extra-framework  $\text{Al}^{3+}$  species, more abundant in Cu- $\beta$  than in Cu-ZSM-5.

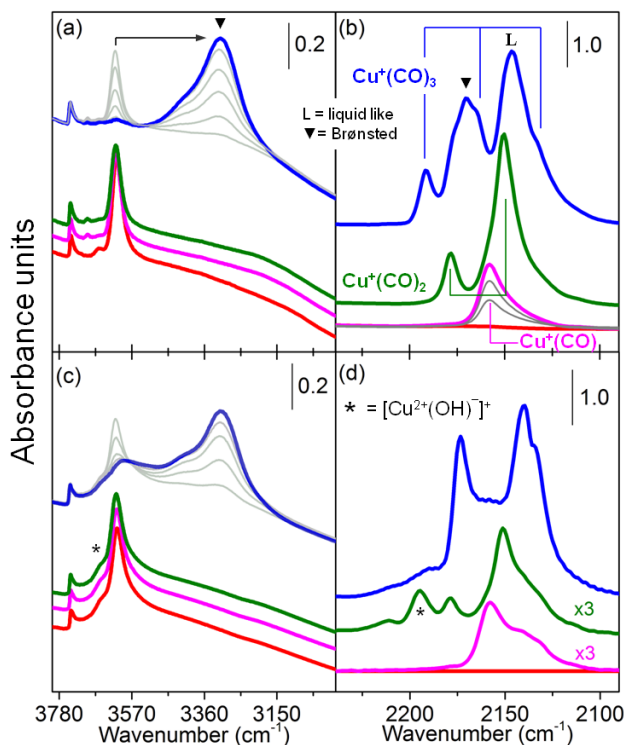


**Fig. 3** As Fig. 2 for Cu-ZSM-5.

**Table 4** C-O,  $\nu_a(\text{CO})_m$  ( $m = 1, 2, 3$ ), stretching frequencies of carbonyl adducts in  $\text{Cu}^+$ -zeolites and supported  $\text{Cu}_2\text{O}$ . When needed, label “a” ( $a = l, m, h$ ) refers to low, medium and high frequency components of the adduct. For  $\text{Cu}_2\text{O}/\text{SiO}_2$  and bulk  $\text{Cu}_2\text{O}$  samples, an interval of frequencies has been reported for  $\nu(\text{CO})$ ,  $\nu_l(\text{CO})_2$  and  $\nu_h(\text{CO})_2$  since the frequency position of the band was pressure dependent.<sup>104</sup> sh = shoulder; N. F. = non formed; N.D. = not detected (because experiments were performed at RT).

Sample	$\tilde{\nu}(\text{CO})$ ( $\text{cm}^{-1}$ )	$\tilde{\nu}_l(\text{CO})_2$ ( $\text{cm}^{-1}$ )	$\tilde{\nu}_h(\text{CO})_2$ ( $\text{cm}^{-1}$ )	$\tilde{\nu}_l(\text{CO})_3$ ( $\text{cm}^{-1}$ )	$\tilde{\nu}_m(\text{CO})_3$ ( $\text{cm}^{-1}$ )	$\tilde{\nu}_h(\text{CO})_3$ ( $\text{cm}^{-1}$ )	Reference
Cu-SSZ-13 <sup>a</sup>	2155	2150	2178	2134	2169	2194	this study
Cu-ZSM-5 <sup>a</sup>	2158	2150	2178	2134 (sh)	2166 (sh)	2192	this study
Cu- $\beta$ <sup>a</sup>	2158, 2153	2152	2180	2134 (sh)	2168 (sh)	2193	this study
Cu-ZSM-5 <sup>b</sup>	2157	2151	2178	2138	2167	2192	8
Cu- $\beta$ <sup>b</sup>	2157	2152	2180	2146	2167	2193	85
Cu-SSZ-13	2154	2151	2178	N.D.	N.D.	N.D.	23
Cu-MOR <sup>b</sup>	2159	2152	2180	2146	2167	2193	83
Cu-MOR <sup>b</sup>	2157	2149	2178	2135 (sh)	2170	2191	109
Cu-Y <sup>b</sup> Site II	2159	2148	2178	2138	2165	2188	66
Site II*	2143	2135	2168				
$\text{Cu}_2\text{O}/\text{SiO}_2$	2132- 2127	2127- 2120	2162- 2154	N.F.	N.F.	N.F.	79,104

<sup>a</sup> The frequency of the  $\nu_a(\text{CO})_m$  bands observed in this work are independent of the activation procedure.

<sup>b</sup> Copper zeolites prepared via stoichiometric gas-phase exchange with  $\text{CuCl}$ , resulting in the atomic ratio  $\text{Cu}/\text{Al} = 1$ .



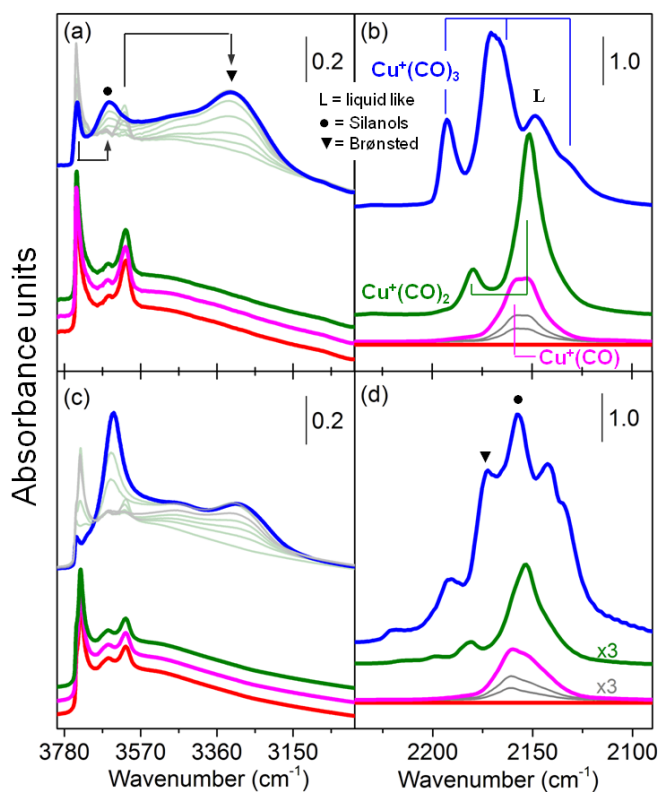


**Fig. 4** As Fig. 2 for Cu- $\beta$ .

Monocarbonyl  $\text{Cu}^+(\text{CO})$  bands obtained in  $\text{O}_2$  treated samples are more complex in both Cu-ZSM-5 and Cu- $\beta$ , showing additional components on the right side of the main bands, in respect to the *vacuum* activated samples (see magenta curves in part b and d of Fig. 3, 4).

The overall comparison between parts (a), (b) and (c), (d) of Fig. 2, Fig. 3 and Fig. 4 clearly shows that significantly different materials are obtained following the *vacuum* or the  $\text{O}_2$  activation procedures, as the population and the ability to coordinate CO molecules of the different sites is modified. This relevant conclusion could not be reached by Szanyi *et al.*,<sup>23</sup> because performing CO adsorption experiments at RT could monitor only the strongest adsorption processes only, *i.e.* the formation of  $\text{Cu}^+(\text{CO})$ ,  $\text{Cu}^+(\text{CO})_2$  and  $\text{Al}^{3+}\cdots\text{CO}$  complexes, the last one ascribed to  $\text{Cu}^{2+}(\text{CO})$  complexes. As the stretching frequencies of  $\text{Cu}^+(\text{CO})$  and  $\text{Cu}^+(\text{CO})_2$  complexes are not affected by the treatment (Table 4), they concluded that IR spectra collected on annealed and oxidized Cu-SSZ-13 samples are essentially identical to those collected on the reduced form of the zeolites.<sup>23</sup>

### 2.3. IR spectroscopy of adsorbed NO

The main difference between CO and NO is that the additional electron in NO occupies the  $\pi^*$ -orbital. This causes a greater NO sensitivity to the electronic state of the cation during formation of the M-NO bond than for CO, since even slight alterations in electron density in this orbital noticeably change the frequency of the NO stretching vibration,  $\nu(\text{NO})$ . Contextually, NO is

traditionally used to probe the oxidation state of copper cations in zeolites, due to its ability to form nitrosyl stable adducts with both  $\text{Cu}^{2+}$  and  $\text{Cu}^+$  cations.<sup>8,60,74,75,97,110,111</sup>

At room temperature, according to Spoto *et al.*<sup>97</sup>, coordination of NO to the  $\text{Cu}^+$  sites and formation of nitrosyls, is combined with decomposition reaction, with initial formation of  $\text{N}_2\text{O}$  and  $\text{Cu}^{2+}(\text{NO})(\text{NO}_2)$  adducts. For this reason, in order to suppress NO decomposition, NO was dosed on the samples cooled by liquid nitrogen. As at NO partial pressure of few mbar  $(\text{NO})_2$  dimers are formed,<sup>8</sup> the experiments were performed by dosing NO in  $10^{-2}$ - $10^{-1}$  mbar interval.

Fig. 5 reports NO adsorption experiments on *vacuum* (parts a,b and c) and  $\text{O}_2$  activated (parts d, e and f) samples. Starting from low NO coverages, *vacuum* activated Cu-SSZ-13 (Fig. 5a) shows a band centred at  $1810\text{ cm}^{-1}$  due to the interaction between NO and isolated  $\text{Cu}^+$  leading to the formation of  $\text{Cu}^+(\text{NO})$  mononitrosyl complexes;<sup>8,60,74,75,97,110</sup> First NO dosages on the sample are reported in the inset of the figure, and clearly show a symmetric and well defined band. By increasing NO coverage, the  $1810\text{ cm}^{-1}$  band evolves in two main components at  $1826$  (with a shoulder at  $1833\text{ cm}^{-1}$ ) and  $1728\text{ cm}^{-1}$  (with a shoulder at  $1742\text{ cm}^{-1}$ ) ascribed as symmetric and asymmetric stretching of  $\text{Cu}^+(\text{NO})_2$  dinitrosyl complexes, respectively.<sup>8,60,74,75,97,110,111</sup> As already observed for Cu-MOR,<sup>85,112</sup> a single NO molecule is able to form similar  $\text{Cu}^+(\text{NO})$  adducts on two slightly different  $\text{Cu}^+$  sites (already detected by  $\text{N}_2$  adsorption, see Fig. 1) but, when a second NO molecule is inserted, the  $\text{Cu}^+(\text{NO})_2$  complexes are able to probe a larger space around the  $\text{Cu}^+$  sites and so to better discriminate among them. The absence of any significant band in the  $1950$ - $1870\text{ cm}^{-1}$  range, where  $\text{Cu}^{2+}(\text{NO})$  complexes are expected, implies that nearly all cupric ions in accessible positions have been reduced to cuprous ions during the thermal activation. This is in line with what already observed for other  $\text{Cu}^{2+}$ -exchanged zeolitic systems.<sup>59,86</sup> Moreover the absence of absorption bands typical of cuprous oxide phase (see Table 5) excludes the formation of these extra species during the high temperature treatment. This observation is only made on the basis of the assignment of the  $2135\text{ cm}^{-1}$  band to monocarbonyl complexes formed on  $\text{Cu}^+$  ions located in constrained environments, see Section 2.2.4. *Vacuum* activated Cu-ZSM-5 and Cu- $\beta$  show approximately the same trend as Cu-SSZ-13, and corresponding mono- and dinitrosyl complexes frequencies are reported in Table 5. In Cu-ZSM-5 the shape of mononitrosyl band at  $1813\text{ cm}^{-1}$  is significantly tailed on the low frequency side suggesting some site heterogeneity, while for Cu- $\beta$  where two components are observed at  $1802\text{ cm}^{-1}$  and  $1815\text{ cm}^{-1}$  (shoulder). Note that very similar features have been observed in case of monocarbonyl bands (see section 2.2. and Fig. 3 -Fig. 4). In both cases, we observe a total conversion of mono-nitrosyl into di-nitrosyl complexes upon increasing the  $P_{\text{NO}}$ . The exact frequencies of the observed nitrosyl complexes are reported in Table 5, together with literature data reported for comparison.

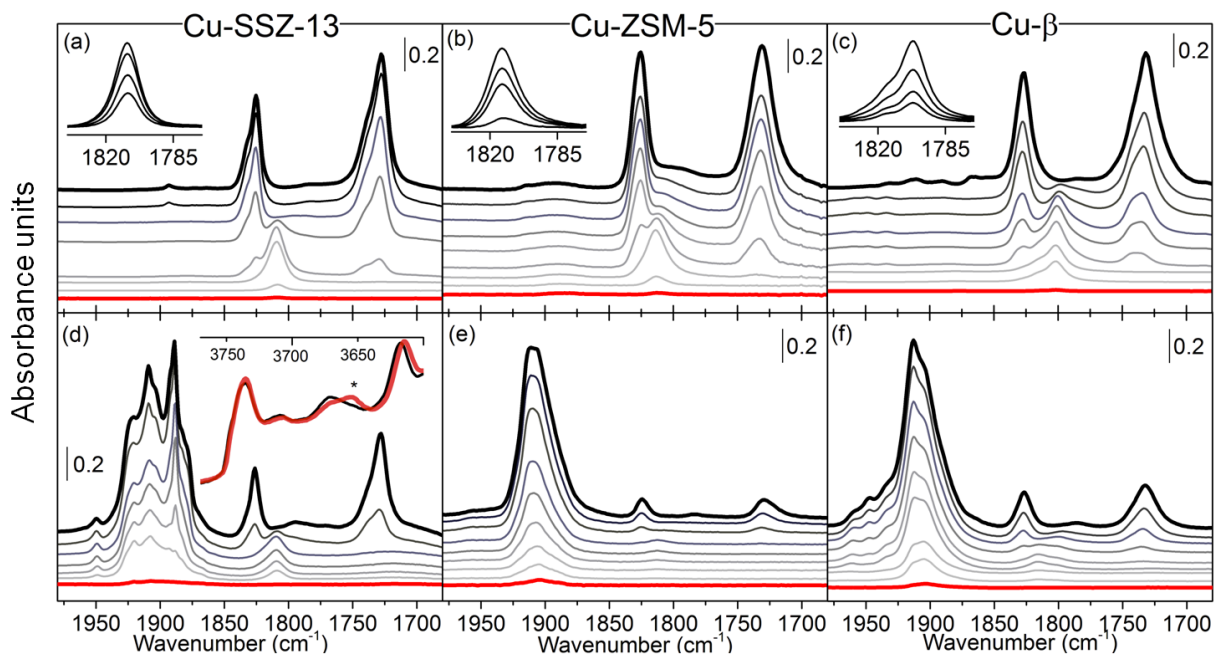


**Fig. 5** Low temperature ( $\sim 100$  K) IR spectra of NO dosed at increasing equilibrium pressure (from  $7 \times 10^{-2}$  to  $7 \times 10^{-1}$  Torr) on Cu-zeolites. Red curves show lowest NO coverage, black curves refer to highest NO coverage, while fading curves refer to intermediate adsorption steps. Upper parts (a), (b) and (c) refers to *vacuum* activated zeolites, showing the  $\text{Cu}^+(\text{NO}) \rightarrow \text{Cu}^+(\text{NO})_2$  evolution; insets report low coverage spectra corresponding to  $\text{Cu}^+(\text{NO})$  complexes. Lower parts (c), (d) and (e) refer to  $\text{O}_2$  activated zeolites showing  $\text{Cu}^{2+}(\text{NO})$  and residual  $\text{Cu}^+(\text{NO})_2$  adducts. Inset in part (d) reports the corresponding bands in the  $\nu(\text{OH})$  region, testifying the erosion of the  $3650 \text{ cm}^{-1}$  band upon formation of NO adducts with dehydrated  $[\text{Cu}-\text{OH}]^+$  species.

As already observed when CO was used as probe (parts d of Fig. 2, Fig. 3 and Fig. 4), despite the presence of oxygen during the thermal treatment, a not negligible amount of  $\text{Cu}^+$  is monitored on the  $\text{O}_2$  activated samples (Fig. 5, parts d, e and f). As already observed during CO adsorption experiments, apart from the intensity, of course decreased, both shape and position of  $\text{Cu}^+(\text{NO})_n$  ( $n=1,2$ ) complexes bands in  $\text{O}_2$  activated sample are approximately equal to those observed on *vacuum* activated samples implying that the  $\text{Cu}^+$  location and distribution are not affected by the presence of oxygen during the thermal treatment. The presence of  $\text{Cu}^+$  ions detected by both CO and NO probes on  $\text{O}_2$  activated samples could be related to several factors: (i) in order to remove all trace of water adsorbed on the zeolites channels and pores, static treatment in presence of  $\text{O}_2$  needed to be alternated by many desorption steps (see Section 5.2) performed under *vacuum* conditions and at relevant high temperature which could lead a substantial reduction of  $\text{Cu}^{2+}$ . (ii) As observed by Szanyi *et al.*<sup>23</sup> on a fully oxidized Cu-SSZ-13,  $\text{Cu}^+$  could be formed by a red-ox charge transfer reaction by the reaction  $\text{Cu}^{2+}(\text{NO}) \rightarrow \text{Cu}^+-\text{NO}^+$ . The latter specie is expected to give an absorption band in the  $2170\text{-}2160 \text{ cm}^{-1}$  region. As we did not observe such band in our experiments, we can exclude that  $\text{Cu}^+$  ions detected in our case could be generated by a similar redox pathway. From all these observations, the only possible  $\text{Cu}^+$  formation detected is related to the activation thermal treatment (points i), allowing us to consider the  $\text{O}_2$  activated samples as partially (and not totally)

oxidized.

**Table 5**  $\nu(\text{N-O})$ , stretching frequencies of mono- and di-nitrosyl adducts in  $\text{Cu}^+$  sites in zeolites and in supported  $\text{Cu}_2\text{O}$ .

Sample (site)	$\tilde{\nu}(\text{NO})$ ( $\text{cm}^{-1}$ )	$\tilde{\nu}_{\text{sym}}(\text{NO})_2$ ( $\text{cm}^{-1}$ )	$\tilde{\nu}_{\text{as}}(\text{NO})_2$ ( $\text{cm}^{-1}$ )	Reference
Cu-SSZ-13 (A)	1809	1826	1728	this study
Cu-SSZ-13 (B)	1809	1833 (sh)	1742 (sh)	this study
Cu-SSZ-13 <sup>a</sup>	1810, 1785 (sh)	N.O.	N.O.	23
Cu-ZSM-5	1813	1730	1825	this study
Cu-ZSM-5 <sup>b</sup>	1812	1734	1827	8
Cu- $\beta$	1802, 1815 (sh)	1828	1734, 1743 (sh)	this study
Cu- $\beta$ <sup>a</sup>	1810	N.O.	N.O.	114
Cu- $\beta$ <sup>b</sup>	1811	1730	1826	85
Cu-MOR <sup>b</sup> (main channel)	1813	1730	1828	74
Cu-MOR <sup>b</sup> (side pocket)	1813	1785	1870	74
Cu-Y <sup>b</sup> (II)	1814	1728	1824	66
Cu-Y <sup>b</sup> site (II*)	1788	N.O.	N.O.	66
$\text{Cu}_2\text{O}/\text{SiO}_2$	1775	1709	1811	79

<sup>a</sup> Experiment performed at RT, thus under NO decomposition conditions.

<sup>b</sup> Copper zeolites prepared via stoichiometric gas-phase exchange with CuCl, resulting in the atomic ratio Cu/Al = 1.

Using CO as probe (parts d of Fig. 2, Fig. 3 and Fig. 4) we learned that  $\text{O}_2$  activated zeolites still contain a fraction of  $\text{Cu}^+$ , however no information was gained on the complementary fraction of copper, besides the presence of dehydrated  $[\text{Cu-OH}]^+$  complexes. Experiments reported in Fig. 5d,e,f tell us that, as expected, a significant fraction is in the +2 oxidation state forming  $\text{Cu}^{2+}(\text{NO})$  adducts adsorbing in the 1970-1850  $\text{cm}^{-1}$  range. The complexity of the absorption features of  $\text{Cu}^{2+}(\text{NO})$  adducts (particularly relevant for Cu-SSZ-13) clearly suggests the presence of different  $\text{Cu}^{2+}$  cationic sites. Deconvolution of the spectra of partially oxidized Cu-ZSM-5 and Cu- $\beta$  (see Fig.S2 in ESI) reveal the presence of three main components at 1912, 1903 and 1895  $\text{cm}^{-1}$  (see Table 6), suggesting at least three different environments for  $\text{Cu}^{2+}$ , where the last is practically negligible in the case of Cu- $\beta$ . Similar band positions are also observed in the case Cu-SSZ-13, which additionally shows a very sharp feature at 1890  $\text{cm}^{-1}$ .

On oxidized Cu-ZSM-5 zeolite Dedecek *et al.*<sup>113</sup> observed two main component at 1895 and 1912  $\text{cm}^{-1}$  (and other less intense at 1921 and 1906  $\text{cm}^{-1}$ ), which were assigned to two different copper sites and they were suggested to be balanced by one and two Al atom, respectively. The band at 1895  $\text{cm}^{-1}$  was assigned to monovalent complex likely to be  $[\text{Cu-OH}]^+$ . Interestingly, this band (observed in our case at 1890  $\text{cm}^{-1}$ ) is strong in Cu-SSZ-13, it's a shoulder in Cu-ZSM-5 and is almost absent in Cu- $\beta$ . Moreover, a very similar intensity trend has been found for: (i) the OH band around 3650  $\text{cm}^{-1}$  on the  $\text{O}_2$  activated samples (parts d of Fig. 2, Fig. 3 and Fig. 4), and (ii) the CO band at 2207  $\text{cm}^{-1}$ , (part d of the same figures). Even more important is the correlations, observed in both CO and NO experiments, between the erosion of the 3650  $\text{cm}^{-1}$  component and the rise of the 2207  $\text{cm}^{-1}$  (CO dosage, Fig. 2c,d) and 1890  $\text{cm}^{-1}$  (NO dosage, Fig. 5d and inset) bands, that gives strong support to the assignment of the 3650  $\text{cm}^{-1}$  band to the  $\nu(\text{OH})$  stretching mode of dehydrated

[Cu–OH]<sup>+</sup>.

**Table 6** N–O stretching frequencies of mono-nitrosyl adducts in Cu<sup>2+</sup> sites in zeolites and in supported CuO. w = weak; m = medium; s = strong; sh = shoulder.

Sample(site)	$\bar{\nu}(\text{NO})$ (cm <sup>-1</sup> )	Reference
Cu-SSZ-13	1950 <sup>w</sup> , 1921 <sup>m</sup> , 1909 <sup>m</sup> , 1904 <sup>m</sup> , 1890 <sup>s</sup>	this study
Cu-SSZ-13 <sup>a</sup> (I)	1920-1880	23
Cu-SSZ-13 <sup>a</sup> (II)	1948,1930	23
Cu-ZSM-5	1912, 1905, 1895 (sh)	this study
Cu-ZSM-5 <sup>a</sup>	1921, 1912, 1906, 1895	113
Cu-ZSM-5 <sup>b</sup>	1890	8
Cu-β	1912, 1903, 1895 (sh)	this study
Cu-β <sup>a</sup>	1896	114
Cu-MOR <sup>a</sup>	1960, 1938, 1921, 1909 <sup>s</sup> , 1895	113
Cu-Y <sup>b</sup> (II)	1955	66
Cu-Y <sup>b</sup> (II*)	1923	66
CuO	1865, 1855	115

<sup>a</sup> Experiment performed at RT, thus under NO decomposition conditions.

<sup>b</sup> Copper zeolites prepared via stoichiometric gas-phase exchange with CuCl, resulting in an atomic ratio Cu/Al = 1.

### 3. UV-Vis-NIR spectroscopy

Since colorless Cu<sup>+</sup> ion has a fully occupied *d* shell (3d<sup>10</sup>), electronic spectra analysis, involving d-d transitions, is only possible for Cu<sup>2+</sup> (3d<sup>9</sup>) systems, *i.e.* hydrated and O<sub>2</sub> activated samples.<sup>40,59,69,86,116-118</sup> Fully hydrated samples have a pale blue color, and corresponding UV-Vis-NIR spectra are shown in Fig. 6. In the low frequency part of the NIR region (inset of Fig. 6) two sharp main features are observed around 7140 cm<sup>-1</sup> and 5260 cm<sup>-1</sup> corresponding to the overtone of the  $\nu$  and to the combination of  $\nu$  and  $\delta$  of physisorbed water, respectively.<sup>119,120</sup> In the high frequency part of the NIR region (inset of Fig. 6) all samples reveal a broad and asymmetric transition centered around 12000 cm<sup>-1</sup>. This band usually appears in hydrated Cu<sup>2+</sup> zeolites, and relates to d-d transition occurring in distorted octahedral aquo complexes of Cu<sup>2+</sup>. The origin of the distortion of cupric octahedral complexes is commonly explained from the crystal field theory as the fivefold degenerated <sup>2</sup>D term is split in an octahedral ligand field. The maximum symmetry configuration of this system with a twofold degenerate ground state is unstable and exhibits the Jahn–Teller effect,<sup>121</sup> causing a splitting of both the ground and excited states. This leads to a distortion of the octahedral Cu<sup>2+</sup> complex, *e.g.* axial elongation of the tetragonal bipyramide of octahedral Cu<sup>2+</sup> complex (Scheme 1). Because of the Jahn–Teller effect, the band at 12000 cm<sup>-1</sup> observed in the fully hydrated zeolites is usually composed by three sub-components at around 12400, 11500 and 10700 cm<sup>-1</sup> corresponding to most probable  $d(xz) \rightarrow d(x^2-y^2)$ ,  $d(yz) \rightarrow d(x^2-y^2)$  and  $d(xy) \rightarrow d(x^2-y^2)$  transitions (Scheme 1).<sup>122</sup> Two main types of Cu<sup>2+</sup> complexes are expected to be present giving an absorption band around 12000 cm<sup>-1</sup>: (i) divalent complexes charge compensated by a pair of nearby Al, *e.g.* [Cu(H<sub>2</sub>O)<sub>6</sub>]<sup>2+</sup> or [Cu–O(L)<sub>6-n</sub>(H<sub>2</sub>O)<sub>n</sub>]<sup>2+</sup> (where O(L) are oxygen

framework atoms coordinated to  $\text{Cu}^{2+}$ ); (ii) “monovalent” complexes charge compensated by one Al atom, *e.g.*  $[\text{Cu}-\text{OH}(\text{H}_2\text{O})_5]^+$  or  $[\text{Cu}-(\text{OH})\text{O}(\text{L})_{5-n}(\text{H}_2\text{O})_n]^+$ . Complexes such as  $[\text{Cu}-(\text{AcO})(\text{H}_2\text{O})_5]^+$  are excluded in our case, since prior to measurements all the samples were intentionally calcined in order to remove residual organic ligands. Although the d-d band at  $12000\text{ cm}^{-1}$  is too broad to discriminate the co-presence of the complexes mentioned above, corresponding edge position provides additional information. In order to better compare the d-d edge position of the three samples normalization to the maxima in the  $12000\text{ cm}^{-1}$  region was performed. A detailed analysis of the spectra reveals the following edge energy order:  $\text{Cu-SSZ-13} > \text{Cu-}\beta \gg \text{Cu-ZSM-5}$ . According to Dedecek *et al.*<sup>123</sup> the edge position is mainly affected by Al distribution which determines the relative concentration of the divalent and “monovalent” complexes mentioned above. Contextually, the presence of one or more ligands with a different electronegativities (*e.g.*  $\text{OH}^-$ , framework oxygen) creating a stronger local field along the x or/and y axis in the complex can result in a considerable increase of the  $d(x^2-y^2)$  orbital energy (see Scheme 1), yielding a more distorted sites and a shift of the absorption band to higher frequencies. From all of these observations it looks like Cu-SSZ-13 reveals the larger distorted  $\text{Cu}^{2+}$  complexes in hydrated form in comparison with Cu-ZSM-5 and Cu- $\beta$ . This is in agreement with the study by Weckhuysen and co-workers where they used EXAFS to analyze Cu-SSZ-13 and concluded that, for the hydrated sample, four oxygen atoms coordinate to the  $\text{Cu}^{2+}$  ion with an average Cu–O distance of  $2.02\text{ \AA}$ ,<sup>28,67</sup> implying an high distortion of the sites.

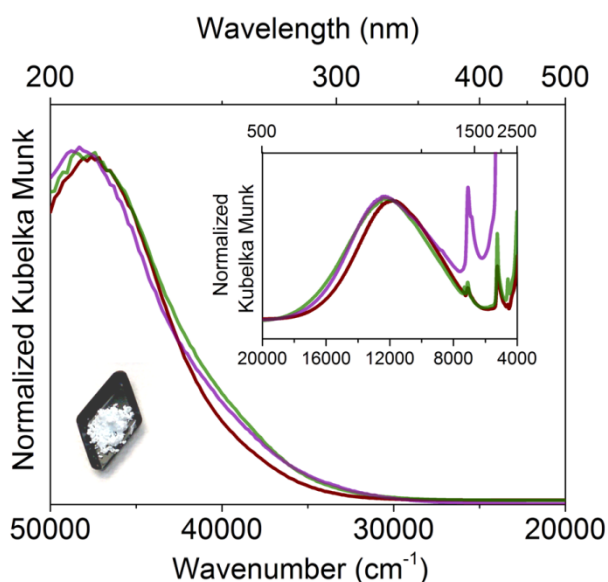
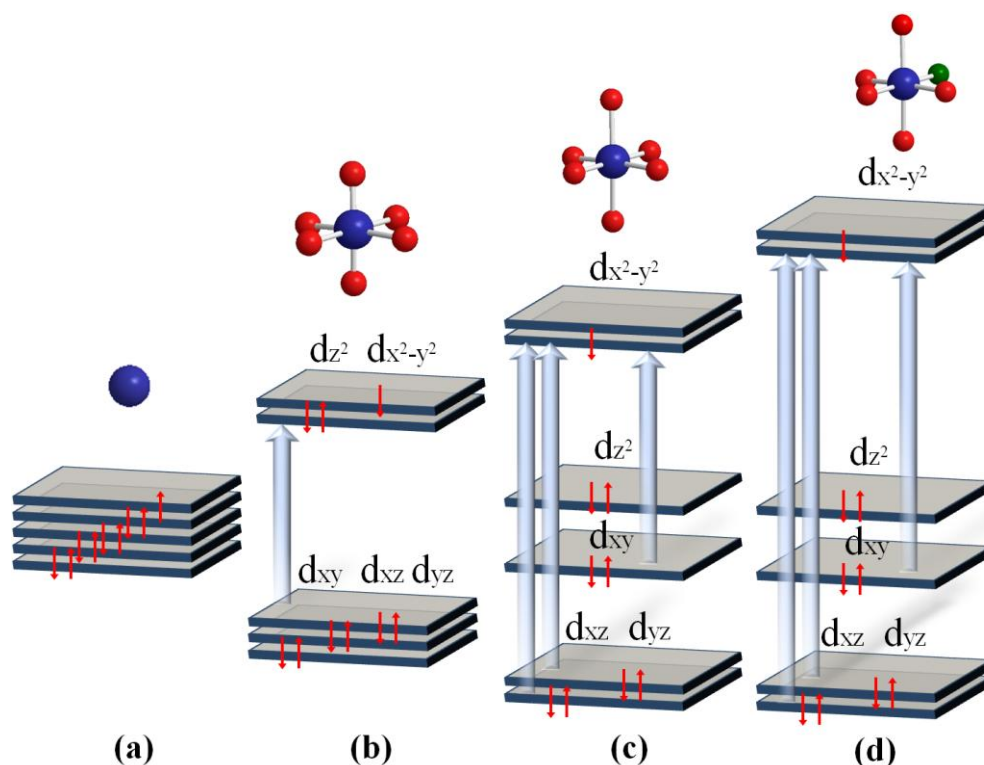


**Fig. 6** UV-Vis-NIR spectra of hydrated Cu-SSZ-13 (green curve), Cu-ZSM-5 (wine curve) and Cu- $\beta$  (purple curve). Charge transfer and d-d transitions are reported in the main part and in the inset, respectively. To allow a direct comparison on the relative differences, spectra have been normalized. Normalization has been performed at the maximum of the d-d band ( $12000\text{ cm}^{-1}$ ) in the inset and at  $48000\text{ cm}^{-1}$  in the main part. A picture of the pale blue powder of Cu-SSZ-13 is also reported. Cu-ZSM-5 and Cu- $\beta$  (not shown) are virtually indistinguishable by eyes from Cu-SSZ-13 in their hydrated forms.

In addition to the absorption band of the d-d transitions, the electronic spectra of  $\text{Cu}^{2+}$  aquo complexes show an intense absorption band centered at around  $48000\text{ cm}^{-1}$  (main part of Fig. 6), which corresponds to a ligand to metal charge transfer (LMCT) transition ( $\text{O}^{2-}\text{Cu}^{2+} \rightarrow \text{O}^-\text{Cu}^+$ ). In the hydrated samples, no accurate comparison between the three frameworks could be made since the intensity of this band is greatly affected by the scattering properties of each material (mainly depending on water content and on the zeolite particle size).



**Scheme 1** Splitting of  $^2D$  term of  $\text{Cu}^{2+}$  ion (blue sphere) in fields of ligands (red and green spheres) in different coordination environments, and corresponding electronic transitions. (a) Spherical coordination (absence of ligands or ideal uniform isotropic ligands). (b) Octahedral coordination. (c) Elongated square bipyramidal coordination and corresponding Jahn–Teller effect.<sup>121</sup> d-orbitals aligned with the two more distant donor atoms along the z-coordinate experience less repulsion leading to a drop in energy ( $d_{xz}$ ,  $d_{yz}$ , and  $d_{z^2}$ ), while those closer to the in-plane donor atoms ( $d_{xy}$ ,  $d_{x^2-y^2}$ ) rise in energy. (d) Distorted elongated bipyramidal coordination due to the effect of a stronger ligand (green ball) likely to be  $\text{OH}^-$  or framework oxygen.

A comparison between hydrated (black line) and  $\text{O}_2$  activated (blue line) samples is reported in Fig. 7. The most relevant d-d and CT bands observed in these spectra are also summarized in Table 7.  $\text{O}_2$  activated Cu-SSZ-13 show a dark blue colour, whereas Cu-ZSM-5 and Cu- $\beta$  appear pale green (see reported photos). The main effects of the activation process on the zeolite spectra can be summarized as follow: (i) total disappearance of water signals in the NIR spectral region, confirming that the de-hydration is complete during the treatment, (ii) a blue shift and increase of the d-d absorption bands, with a pronounced split phenomena in the case of Cu-SSZ-13, and (iii) a red shift of the LMCT maximum, which now appear in the  $42000\text{--}40000\text{ cm}^{-1}$  range, together with the appearance of new CT bands at lower energies in the  $32000\text{--}22000\text{ cm}^{-1}$  range. All of these changes can be ascribed to decomposition of the aquo complexes, which induces the removal of water from the first coordination sphere of  $\text{Cu}^{2+}$ . Furthermore, removal of the water ligands allows

the  $\text{Cu}^{2+}$  cations to interact (stronger) with framework oxygen atoms and to be stabilized in a stronger distorted local environment. The replacement of water by oxygen framework atoms is evidenced by the red shift of the LMCT maximum. Water as a ligand also lies at the very beginning of the nephelauxetic series,<sup>124</sup> and thus makes very ionic coordination bonds. The red shift of the LMCT band is a clear indication of an increase in the degree of covalency in the ligand to -metal bond. Moreover, the high tetragonal distortion of the new sites is testified by the corresponding magnification of the d-d transition intensities, becoming less Laporte forbidden than the more centrosymmetric  $\text{Cu}^{2+}$  sites in the hydrated systems.<sup>59,86</sup> Furthermore, a blue shift of the d-d band observed on the Cu-SSZ-13 spectrum testifies to a higher *d-d*- splitting suggesting the presence of highly distorted  $\text{Cu}^{2+}$  sites, as already observed in the corresponding hydrated system (see Scheme 1d, where some ligands are substituted by coordination vacancies).

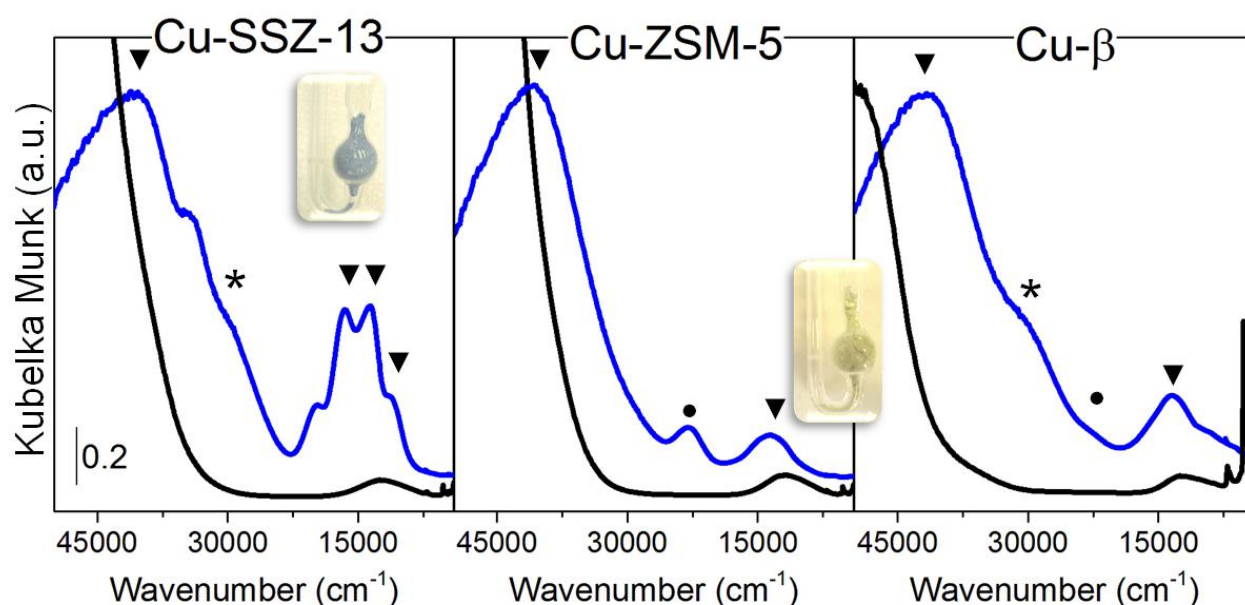


**Fig. 7** Comparison between UV-Vis-NIR spectra of hydrated (black line) and  $\text{O}_2$  activated (blue line) Cu-zeolites. Photographs of the  $\text{O}_2$  activated powders are also reported in order to show the visual differences: Cu-SSZ-13, dark blue; Cu-ZSM-5 pale green. The color of  $\text{O}_2$  activated Cu- $\beta$  (not reported) is as that of Cu-ZSM-5. See Table 7 for the quantitative values of the main CT and d-d bands. Spectra are not normalized. Markers are also reported as an attempt of assignment to the observed bands: ▼ = isolated  $\text{Cu}^{2+}$  ions, ● =  $[\text{Cu}-\text{O}-\text{Cu}]^{2+}$  dimers, \* =  $[\text{Cu}_2(\mu-\eta^2:\eta^2-\text{O}_2)]^{2+}$  dimers.

It is generally accepted that the most favorable crystallographic sites of isolated  $\text{Cu}^{2+}$  in de-hydrated zeolites are those located in the plane or slightly above the plane of the framework oxygens in six-membered rings (6MRs).<sup>30,69</sup> The geometry of these sites is highly affected by the presence of one or two Al atoms in close vicinity. For example, 3-, 4- and even 5-fold coordination with different geometry have been postulated for  $\text{Cu}^{2+}$  ions in de-hydrated Cu-ZSM-5 depending on both the cationic position and the number of neighboring Al.<sup>69,125,126</sup> For each site a specific electronic diagram of d-orbitals is expected, being difficult to identify every singular electronic contribution especially in those systems where many species and locations exist. Conversely Cu-SSZ-13 seems

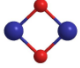
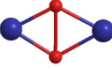
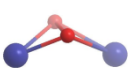
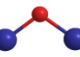
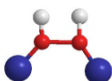


to have a unique geometry and location for isolated  $\text{Cu}^{2+}$  in the double six rings units, which tend to locate off the plane of 6MRs to maintain close coordination with three lattice oxygen (average Cu-O distances of 1.93Å) in a square planar coordination.<sup>27,28,67</sup>

**Table 7** d-d and CT transitions of  $\text{Cu}^{2+}$  species in hydrated and  $\text{O}_2$  activated zeolites ( $\text{O}_2/\text{He}$  50 % v/v at 400°C). Values obtained from the spectra reported in Fig. 7.

	d-d transition ( $\text{cm}^{-1}$ )		CT transition ( $\text{cm}^{-1}$ )	
	Hydrated	$\text{O}_2$ activated	Hydrated	$\text{O}_2$ activated
<b>Cu-SSZ-13</b>	~ 12000	19700, 16500, 13600, 11000	~ 48000	40500, 32000 (sh), 29000 (sh)
<b>Cu-ZSM-5</b>	~ 12000	13500	~ 48000	41000, 22700
<b>Cu-β</b>	~ 12000	13500, 8800 (sh)	~ 48000	41800, 30000 (sh), 22700 (sh),

**Table 8** Electronic absorption features of some copper pairs.  $k_{max}$  refers to the maximum of the absorption.

			$k_{max}$ ( $\text{cm}^{-1}$ )	Ref.
<b><math>[\text{Cu}_2(\mu\text{-O})_2]^{2+}</math></b> <i>Bis(μ-oxo)dicopper</i>			32700-30800 25000-22300	131
<b><math>[\text{Cu}_2(\mu\text{-}\eta^2\text{:}\eta^2\text{-O}_2)]^{2+}</math></b> <i>Bis(μ-η<sup>2</sup>: η<sup>2</sup> peroxo)dicopper</i>	planar		29600-27300 19700-17000	131
	bent		~ 27800 23800-20400 ~ 18200	
<b><math>[\text{Cu}_2(\mu\text{-O})]^{2+}</math></b> <i>Mono(μ-oxo)dicopper</i>			22700	37,128,132
<b><math>[\text{Cu}_2(\mu\text{-OH})_2]^{2+}</math></b> <i>Bis(μ-hydroxo)dicopper</i>			32000-30000	133,134

The formation of  $\text{Cu}^{2+}$  oxygen-bridged pairs occurring at high temperature in the presence of oxygen has to be taken into account, making the assignments of the observed bands less straightforward. The spectrum of  $\text{O}_2$  activated Cu-ZSM-5 exhibits a peculiar tail at 22700  $\text{cm}^{-1}$  (also present but with lower intensity in the Cu-β spectrum), suggesting at least one different Cu specie in addition to isolated  $\text{Cu}^{2+}$  ions. As proven in several works from the Schoonheydt group,<sup>117,127,128</sup> this last band is related to the formation of mono(μ-oxo)dicopper, *i.e.*  $[\text{Cu-O-Cu}]^{2+}$  bridges, whose oxygen do not belong to the zeolite framework. Conversely,  $[\text{Cu-O-Cu}]^{2+}$  dimers are excluded to form in  $\text{O}_2$  activated Cu-SSZ-13 since no band at 22700  $\text{cm}^{-1}$  was found on the corresponding spectrum. This is an important conclusion, because even if Cu and Al contents would be high enough to favour the formation of  $\text{Cu}^{2+}$  dimers, as in the case of Cu-ZSM-5 and Cu-β, their absence in CHA framework clearly suggest a peculiar framework effect on  $\text{Cu}^{2+}$  speciation. An explanation of this last phenomena could be related to the close vicinity of two particular Cu sites, probably too far away in the case of Cu-SSZ-13 to allow the mono(μ-oxo)dicopper formation if compared with

Cu-ZSM-5 and Cu- $\beta$ .<sup>62,129</sup> Consider that from both DFT calculation and EXAFS analysis the typical distance between Cu-Cu in  $[\text{Cu-O-Cu}]^{2+}$  dimers has been estimated to be around 3.29 Å in Cu-ZSM-5.<sup>128</sup> The presence of other kind of copper pairs *e.g.* where the distance between two  $\text{Cu}^{2+}$  ions is higher, could be not ruled out due to the presence of complex absorption bands in both the CT and d-d region in the Cu-SSZ-13 spectrum (also observed in the case of Cu- $\beta$ , see asterisk in Fig. 7). For sake of comparison, typical absorption bands of some copper pairs observed in common synthetic model complexes, also suggested to exist in Cu-ZSM-5 from theoretical calculations<sup>39,130</sup> is reported in Table 8. From these values it is clear that band positions of such complexes are in close proximity to those detected in Cu-SSZ-13 (see Table 7), and an assignment could be endeavoured. One of the possible candidates seem to be planar bis( $\mu$ - $\eta^2$ :  $\eta^2$  peroxy)dicopper complex, showing electronic transitions in a range where Cu-SSZ-13 bands appear at 29000 and 19700  $\text{cm}^{-1}$ . However, for a definitive identification, further characterization tools of  $\text{O}_2$  activated Cu-SSZ-13 are needed in order to look into the electronic properties of these Cu-oxo complexes. In this regard, Raman spectroscopy could be very useful and has earlier been useful in identifying  $[\text{Cu-O-Cu}]^{2+}$  dimers in Cu-ZSM-5.<sup>128</sup>

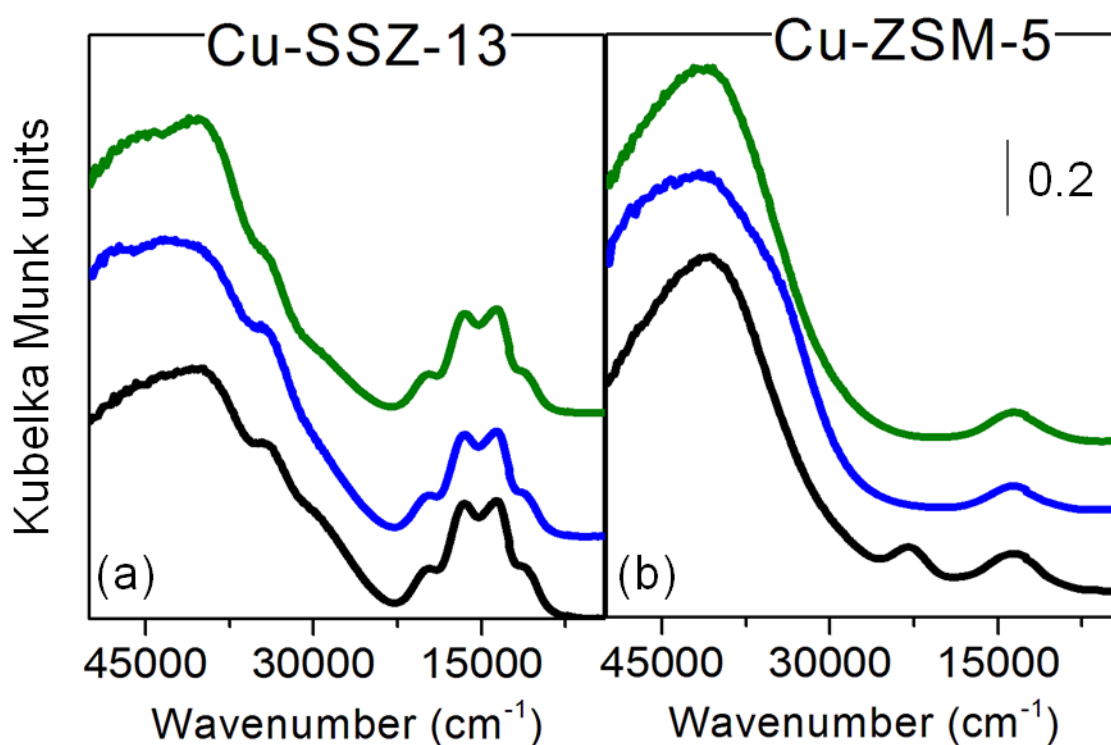


**Fig. 8** DRS UV-Vis-NIR spectra recorded at room temperature on  $\text{O}_2$  activated Cu-SSZ-13 and Cu-ZSM-5 treated in different conditions, parts (a) and (b), respectively. Black lines refer to starting  $\text{O}_2$  activated samples ( $400^\circ\text{C}$ , 2 hours, flow of  $\text{O}_2/\text{He}$  50% v/v). Blue lines refer to samples subsequently treated 1 hour at  $350^\circ\text{C}$  in a flow of 500 ppm  $\text{NO}/10\%$   $\text{O}_2$ . Green lines refer to samples subsequently treated one hour at  $350^\circ\text{C}$  in a flow of 500 ppm  $\text{NH}_3/500$  ppm  $\text{NO}/10\%$   $\text{O}_2$ .

As already mentioned, colours of  $\text{O}_2$  activated Cu-ZSM-5 and Cu- $\beta$  turn pale green, which we believe to be related to the formation of such dimeric species. In fact, whether under  $\text{NO}$  oxidation

(500 ppm NO, 10% v/v O<sub>2</sub>, blue curve in **Error! Reference source not found.b**) or NH<sub>3</sub>-SCR conditions (500 ppm NH<sub>3</sub>, 500 ppm NO, 10% v/v O<sub>2</sub> green curve in **Error! Reference source not found.b**), the total disappearance of the band at 22700 cm<sup>-1</sup> is accompanied by the fading of the pale green colour to an intense blue colour. The collapse of the band at 22700 cm<sup>-1</sup> should be related either to the consumption of [Cu–O–Cu]<sup>2+</sup> as active sites or to their low stability in presence of reactive molecules (NO, NH<sub>3</sub>). Noteworthy the colour of O<sub>2</sub> activated Cu-ZSM-5 and Cu-β in static conditions for IR measurements was intense blue in both cases, suggesting the suppression of the dimeric species during the *vacuum* steps needed to de-hydrate the zeolites. For comparison Cu-SSZ-13 turns dark blue after oxidative treatment, (the colour and respective bands persist even under high temperature reaction conditions treatment, see blue and green curves in **Error! Reference source not found.a**) and reasonably no absorption bands are observed in the 25000-20000 cm<sup>-1</sup> range, excluding the formation of [Cu–O–Cu]<sup>2+</sup> dimeric species in this sample. In conclusion, from UV-Vis-NIR analysis on O<sub>2</sub> activated Cu-SSZ-13, there are no evidence of mono(μ-oxo)dicopper formation, ruling out this species as an NH<sub>3</sub>-SCR active site in this material. In the d-d region, the sharp and well resolved quadruplet, together with the shoulder CT bands at 32000 and 29000 cm<sup>-1</sup> are very peculiar but difficult to be assigned: they could refer either to isolated highly distorted Cu<sup>2+</sup> sites (likely perturbed by the presence of one or two Al atoms) or to the formation of planar bis(μ-η<sup>2</sup>: η<sup>2</sup> peroxo)dicopper complex as shown in Table 8.

#### 4. EPR spectroscopy

Cu<sup>2+</sup> is a paramagnetic ion with one unpaired electron. This allows us to directly probe the copper sites in the substituted zeolites by electron paramagnetic spectroscopy (EPR). Isolated tetragonal Cu<sup>2+</sup> species give a strong EPR response which can be detected both at low temperatures but also at room temperature or operando conditions for the catalysts. The information obtainable by EPR is the symmetry and the coordination sphere of the Cu<sup>2+</sup> centre and a quantification of the amount of EPR active Cu<sup>2+</sup> species.

In this study we are aiming at quantifying the EPR active centres and to compare our findings directly with the IR and UV-Vis-NIR experiments. The same O<sub>2</sub> activation as described in Section 3 was also performed on the samples while in the quartz EPR tube. The samples were furthermore kept under the same atmosphere during measurement at room temperature.

##### 4.1. EPR of hydrated samples

The experimental spectra are shown in Figure 9. By comparison to copper(II) sulphate solid

solutions (not shown) it was possible to quantify the amount of  $\text{Cu}^{2+}$  from the EPR signal with an uncertainty of <10 % as compared to quantification by ICP. The intensity (found as the double integral) of the EPR signal of the fully hydrated samples corresponds well with the total amount copper present in all the zeolite systems corroborating that all copper is in the +2 state. The spectrum of hydrated Cu-SSZ-13 is in complete accordance with Gao *et al.*<sup>24</sup> In the fully hydrated zeolite a significant fraction of the copper is able to detach from the framework and obtain full rotational freedom and a corresponding isotropic EPR signal. This is most clearly seen in the position of the negative peak in the high field part of the EPR spectrum where the isotropic signal and the perpendicular part of the anisotropic signal peak at different field values. For Cu-SSZ-13 and to a lesser extent Cu- $\beta$ , this gives rise to two distinct peaks in the completely hydrated samples (black spectra in Fig. 9). This interpretation was confirmed by obtaining the EPR spectrum of Cu-SSZ-13 after drying in a flow of dry air at room temperature for 32 hours. The isotropic peak disappears without loss of total EPR intensity.

#### 4.1. EPR of $\text{O}_2$ activated samples

In good agreement with the observations from the UV-Vis-NIR experiments the Cu-SSZ-13 attained a dark blue colour whereas Cu-ZSM-5 and Cu- $\beta$  appeared with a paler green colour after the  $\text{O}_2$ -activation. The EPR signals of the activated samples are broader than other EPR spectra reported on copper zeolites<sup>40,55,59,62,125</sup> due to interactions with paramagnetic  $\text{O}_2$  molecules. This prevents us from a detailed analysis of individual copper sites which would be possible after high-vacuum treatments. On the other hand our quantification experiments are not complicated by possible reduction due to the vacuum treatment.

After  $\text{O}_2$  activation at 400°C the intensity decrease to a third of the initial intensity for Cu-SSZ-13 and for Cu-ZSM-5, but is only reduced to ~70 % for Cu- $\beta$  (**Error! Reference source not found.**). At the same time the spectra shift to become only anisotropic and in the case of Cu-SSZ-13 and Cu-ZSM-5 the parallel peaks are resolved.

In order to characterise the activated state further and to extract the g-values and hyperfine coupling constants to compare with the literature, we proceeded to model the EPR spectra with a spin Hamiltonian model. In the case of a tetragonally elongated coordination environment (Scheme 1), the unpaired electron is in a  $d(x^2-y^2)$  orbital. The spin Hamiltonian models the Zeeman effect: The development of the energy levels in the ground state as a function of the magnetic field,  $B$ . The parameters in the model are:  $g_{\parallel}$  and  $g_{\perp}$ , the parallel and perpendicular electronic g-values, and  $A_{\parallel}$  and  $A_{\perp}$ , the parallel and perpendicular hyperfine coupling between the unpaired electron and the nuclear spin on copper (both isotopes  $^{63}\text{Cu}$  and  $^{65}\text{Cu}$  have  $I = 3/2$ ). The experimental spectra in

Figure 9 have been simulated with a simple spin Hamiltonian ( $S = 1/2, I = 3/2$ ):

$$H = g_{\parallel} \mu_B S_z B_z + g_{\perp} \mu_B (S_x B_x + S_y B_y) + A_{\parallel} S_z I_z + A_{\perp} (S_x I_x + S_y I_y) \quad (1)$$

and averaged over a random distribution of crystallites. The best fit parameters using this model are collected in **Error! Reference source not found.**  $A_{\perp}$  is not resolved in the simulated spectra, but is estimated to be below 40 MHz for all samples since the splitting of the perpendicular peak is below the line width. The spin-Hamiltonian parameters are very similar for the zeolites in this investigation and correspond well with a rough average of literature values for individual sites in a range of different dehydrated Cu-zeolites measured by different groups<sup>40,55,59,62,125</sup> corresponding to 5- or 6-coordinated copper centres with oxygen donor ligands. The line width is also fitted and is between 120 and 55 G, large for Cu- $\beta$ , intermediate for Cu-ZSM-5 and smaller for Cu-SSZ-13. The activated Cu- $\beta$  had too low resolution to determine the spin Hamiltonian parameters, but the same parameters as the other two gives reasonable fits. The very high line width for dehydrated Cu- $\beta$  cannot be explained only by interactions with O<sub>2</sub> since this was constant for all samples. A pronounced distribution in the coordination environment of EPR-active copper must be present in Cu- $\beta$  compared to the other zeolites after O<sub>2</sub> activation.

When the Cu-zeolites are left at ambient conditions for several days almost all of the intensity (>90 %) is recovered for all three samples and they turn pale blue again. At first the spectra retains the axial anisotropy of the activated state and the same parameters can be used to fit the EPR of the partially rehydrated samples. With time the spectra obtain a higher percentage isotropic character. The first water molecules after rehydration coordinate to Cu and makes isolated EPR active Cu<sup>2+</sup> sites, but it takes longer for the fully hydrated zeolite to form. An activation cycle was run again for all samples. The EPR intensity is consistently lower (~20%) for the samples after the second activation compared to the first, but all intensity is again recovered by rehydration under ambient conditions.

**Table 9** Spin Hamiltonian parameters used in the simulated spectra given in Fig. 9 and relative intensity of the EPR signal as determined by double integral of the background-corrected first derivative spectra.

	<i>Spin Hamiltonian parameters</i>			<i>Intensity</i> <sup>c</sup>	
	$g_{\parallel}$	$g_{\perp}$	$A_{\parallel}$	<i>hydrated</i> <sup>a</sup>	<i>activated</i>
<b>Cu-SSZ-13</b>	2.355(5)	2.073(5)	450(10) MHz	100 %	35 %
<b>Cu-ZSM-5</b>	2.330(5)	2.073(5)	430(10) MHz	100 %	32 %
<b>Cu-<math>\beta</math></b>	(2.35) <sup>b</sup>	(2.07) <sup>b</sup>	(440 MHz) <sup>b</sup>	100 %	70 %

<sup>a</sup> The intensity of the initial hydrated state is defined to be 100 %. <sup>b</sup> The line width for Cu- $\beta$  was too high to be able to determine the spin Hamiltonian parameters from this spectra alone. The simulated spectrum in Fig. 9 was calculated using the given parameters. <sup>c</sup> The uncertainty on the values of EPR signal intensities should not be underestimated. It is probably at least 10-20 % despite attempts to keep experimental parameters the same.

The loss of EPR intensity in Cu-zeolites upon heating is also found by other authors and has been assigned to the generation of different species: Cu<sup>+</sup>, [Cu-O]<sup>+</sup>, [Cu-O-Cu]<sup>2+</sup> and [Cu<sub>2</sub>( $\mu$ - $\eta^2$ :  $\eta^2$ -

$O_2]^{2+}$ , or to fast relaxing low symmetry  $Cu^{2+}$  species.<sup>135</sup> With the accumulated evidence on which oxidation states are present under such oxidizing conditions as used by us in the activation procedure on a sample not subjected to vacuum and carefully calcined in air previous to the experiments, we believe it is safe to exclude  $Cu^+$  as the EPR silent species in the bulk all three zeolite systems. When performing *in situ* experiments at elevated temperatures under flow conditions (results not shown) the signal intensity is very dependent on whether dioxygen is present or not, but the loss of intensity is always present and is more than the loss of intensity due to the Boltzmann distribution. The  $\mu$ -oxo  $Cu^{2+}$  dimer observed in Cu-ZSM-5 was only estimated to represent 5 % of the total Cu content in a Cu-ZSM-5 with a similar Si/Al ratio of 12.<sup>40,69,128</sup> Since we observe a loss of 65 % of the signal in this sample clearly other EPR silent species must be present as well. When subjected to traces of water at RT all the EPR silent species becomes again EPR active and the colour goes back to pale blue.<sup>59,124</sup> Probably the interaction with water is accompanied by copper centres letting go of framework oxygen atoms and gradually moving into the large cages of the zeolite.<sup>30</sup> This is also in correspondence with the disappearance of the 22700  $cm^{-1}$  line in UV-Vis after exposure to various adsorbates.

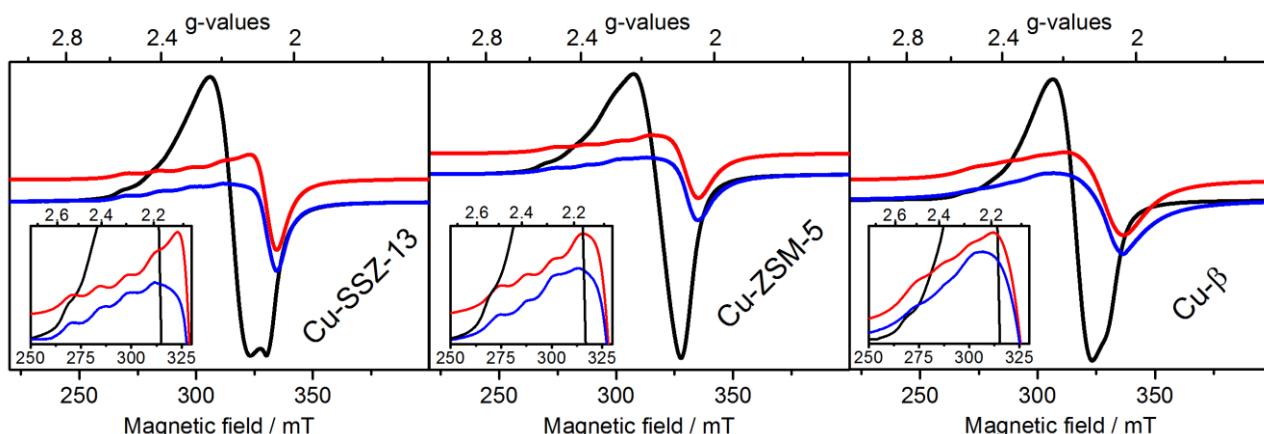


**Fig. 9** EPR spectra of fully hydrated samples are plotted as black lines,  $O_2$  activated samples are plotted as blue lines. The spectra of the activated samples have been simulated with a spin Hamiltonian model with the parameters given in Eq. (1) of the main text. The simulated spectra are plotted as red lines and have been shifted slightly to allow comparison. All experimental spectra have been corrected by subtracting a spectrum of the empty EPR tube measured with exactly the same parameters. The insert is an expansion of the spectral region showing the four parallel peaks.

Antiferromagnetic interactions in  $Cu^{2+}$  dimers provide a diamagnetic ground state and a triplet excited state, which in the case of strong coupling will be high enough in energy not to be populated at RT. Even if the coupling is weak and the triplet states are partially populated the EPR signal from the triplet state can be too broadened to observe. The decrease in EPR intensity upon  $O_2$ -activation was very different for Cu-ZSM-5 and Cu- $\beta$  even though the colours of the dehydrated phases are similar and some EPR silent  $\mu$ -oxo  $Cu^{2+}$  dimers must be present in both. The reason for this is not clear presently, but maybe the local symmetry in the zeolite or the larger percentage of defects in  $\beta$ -zeolite<sup>136</sup> provide copper with more sites where it is able to maintain a comfortable high

coordination number without bridges or close interactions with nearby copper atoms. A broad distribution of EPR active sites could give rise to the more pronounced line broadening observed in the activated Cu- $\beta$  sample.

Maybe surprisingly, the reduction in the intensity of the EPR signal for Cu-ZSM-5 and Cu-SSZ-13 is similar despite the different UV-Vis-NIR spectrum of the activated phases and despite that Cu-ZSM-5 is known to contain oxo-bridged dimers and Cu-SSZ-13 being claimed to have almost exclusively monomers. The main attempt at explaining loss of EPR intensity of seemingly isolated copper sites in Cu-ZSM-5 is done by Lo Jacono *et al.*<sup>135</sup>. Isolated Cu<sup>2+</sup> sites with low symmetry are suspected to be EPR silent due to fast relaxation. No obvious precedent is found for this argument in EPR of copper proteins or coordination compounds with well-defined even highly distorted Cu<sup>2+</sup> coordination environments although sometimes lower temperatures are necessary. On the other hand, EPR signals from more distorted sites are suspiciously absent from the visible EPR signal lending credence to this argument also for Cu-SSZ-13. After activation at temperatures above 400°C Lo Jacono *et al.*<sup>135</sup> found evidence of magnetic interactions in their Cu-ZSM-5 sample. Since the interaction diameter with respect to electronic spin is likely to be longer than what is visible by EXAFS, species suggested to be isolated by EXAFS might be interacting according to EPR and magnetic susceptibility investigations. The isolated Cu<sup>2+</sup> species in Cu-SSZ-13 as advocated by the Richland and Utrecht groups might have long but still electronically relevant interactions after high temperature activations. The reduction of an isolated Cu<sup>2+</sup> during the ammonia SCR reaction has been postulated to be part of the catalytic process and the subsequent reoxidation of the Cu<sup>+</sup> with dioxygen is suggested to close the catalytic cycle.<sup>137</sup> Two or more copper centres close enough to be able to interact electronically are better equipped to handle multi-electron reduction of a dioxygen molecule compared to completely isolated copper centres. Some of the candidates for relative long range interactions in Cu-SSZ-13 are: (i) two copper atoms in 6-membered ring on opposite sides of the same hexagonal prism (Cu-Cu distance 3.8 – 4.3 Å). (ii) One copper in a 6-membered ring and a more mobile copper on a four-membered ring in the wall of the large pores. (iii) Two nearest neighbour 6-membered ring sites in neighbouring large pores (estimated Cu-Cu distance 7 Å). For number (i) and (iii) the copper atoms are not in the same pore channel and this should prevent them efficiently from joining up and making oxo-bridged dimers or oxide phases during harsh hydrothermal treatments.

Summarizing, these data complement the two previous EPR works on Cu-SSZ-13<sup>24,33</sup> only appearing this year. Gao *et al.*<sup>24</sup> focused exclusively on hydrated samples, while Ma *et al.*<sup>33</sup> did not go into detail with the parameters or the intensity loss. In this study, we shows how EPR investigations, together with UV-Vis and IR, can be used to focus on the differences between the

copper sites on the molecular scale despite all external parameters (Si/Al ratio, Cu/Al ratio, activation procedures) being the same. It has been found that Cu-SSZ-13 follows the loss of EPR intensity observed in Cu-ZSM-5 even though the UV-Vis spectra are very different. Conversely, Cu- $\beta$  deviates from both Cu-ZSM-5 and Cu-SSZ-13 despite the UV-Vis spectra of Cu- $\beta$  being similar to Cu-ZSM-5. In conclusion we have identified an activation and measurement protocol that focus on differences in the local Cu coordination symmetry and identifies the spectroscopic fingerprint of a dark blue Cu<sup>2+</sup> species in Cu-SSZ-13 that persists even at high temperatures and after exposure to SCR conditions.

## 5. Experimental section

### 5.1 Preparation of Cu<sup>2+</sup>-exchanged zeolites

Parent  $\beta$  and ZSM-5 were obtained from commercial zeolites. SSZ-13 was prepared from an unseeded reaction mixture with the following composition:



in a method very similar to the one reported in<sup>138,139</sup> where TMdaOH is the template N,N,N-trimethyladamantammonium hydroxide. The gel was prepared by dissolving aluminum isopropoxide ( $\geq 98\%$ , Aldrich) in tetraethyl orthosilicate ( $\geq 99\%$ , Aldrich) followed by adding template solution (25 wt. %, Sacchem INC) slowly. The solution was then stirred mechanically until all products were hydrolyzed. Afterwards hydrofluoric acid (48 wt. %,  $\geq 99.99\%$ , Sigma-Aldrich) was added and again homogenized under mechanical stirring. Finally water was evaporated at 60°C to reach the desired ratio as given in (2).

The resulting gel was then heated under rotation for 3 days at 150°C in a Teflon-lined steel autoclave, recovered by suction filtration, washed with plenty of demineralized water and dried at 100°C. To remove the template, the zeolite was calcined at 580°C for 3 h prior to ion exchange.

Aqueous Cu<sup>2+</sup> ion exchange of the parent materials was carried out with a copper(II)acetate solution (250 mL/g<sub>zeolite</sub>) at different concentrations in order to obtain a final copper content as similar as possible: 3mM, 5mM, 10 mM for Cu-SSZ-13, Cu- $\beta$  and Cu-ZSM-5 respectively. The slurry was continuously stirred for 24 h at room temperature and the exchanged zeolites were recovered by suction filtration, dried overnight at 100°C and further calcined at 500°C in static air for 3 h in order to remove the residual ligand (*i.e.* acetate CH<sub>3</sub>CO<sub>2</sub><sup>-</sup>).

Elemental composition (Table 1) of each sample was determined using inductively coupled plasma optical emission spectroscopy (ICP-OES) on acid digested samples using a Perkin Elmer Optima 7300 DV instrument.



## 5.2. Zeolite pre-treatments before IR measurements

In order to study how different pre-treatment conditions could affect distribution and oxidation state of adsorption centres, two main activation procedures were adopted prior to IR adsorption experiments:

- 1) The first adopted method is labelled *vacuum* activation procedure, and it consists in a treatment of the zeolite under dynamic high *vacuum* conditions ( $p < 10^{-4}$  mbar) at 400°C for 2 hr. After this kind of treatment, a high concentration of  $\text{Cu}^+$  is expected due to the so called “self-reduction” of copper which typically occurs under these conditions.
- 2) The second adopted method is labelled  $\text{O}_2$  activation procedure, *i.e.* oxidative activation procedure, due to the presence of oxygen during the high temperature treatment; it could be schematically described as follow: a) evacuation at room temperature for 30 min; b) heating up to 150°C in static  $\text{O}_2$  atmosphere (100 mbar, 15 min isotherm), followed by short evacuation at 150°C; c) heating up to 250°C in  $\text{O}_2$  atmosphere (100 mbar, 15 min isotherm), followed by short evacuation at 250°C; d) heating up to 400°C in  $\text{O}_2$  atmosphere (100 mbar, 60 min isotherm); e) cooling down the system at 150°C followed by 40 min evacuation step. The evacuation steps are needed in order to remove pre-adsorbed water molecules onto zeolite channels; meanwhile, one should has to take in account that the time and the corresponding temperature of each evacuation steps determine the  $\text{Cu}^{2+}/\text{Cu}^+$  ratio. It has to be mentioned that the treatment just described has been performed in static conditions, whereas for the UV-Vis-NIR measurements and the EPR measurements (see below) the measurement was performed under flow conditions (50% v/v  $\text{O}_2/\text{He}$ ).

## 5.3. Methods

### 5.3.1 FTIR spectroscopy

For IR measurements, thin self-supporting wafers of each zeolite were prepared and placed inside an IR cell designed to allow *in situ* high temperature treatments, gas dosage, and low-temperature measurements. Prior to adsorption experiments samples were pre-treated as describe in Section 3.2. The IR spectra were recorded at  $2\text{ cm}^{-1}$  resolution on a Nicolet 6700 FTIR spectrometer equipped with an mercury cadmium telluride (MCT) cryodetector. For all samples, the spectrum before the gas dosage ( $\text{N}_2, \text{CO}$  and  $\text{NO}$ ) was used as background and all the IR spectra reported, except those reported in  $\nu(\text{OH})$  stretching modes region, are background subtracted. All the adsorption experiments were performed at low temperature: although the IR cell was permanently cooled with liquid nitrogen, the actual sample temperature (under the IR beam) was likely to be *ca.* 100 K. In order to have the possibility to compare band intensities within the full set of spectra, a

normalization to the overtone modes in the 1750–2100  $\text{cm}^{-1}$  region has been performed. Special care has been devoted to follow the same activation procedure for all the samples.

### 5.3.2 UV-Vis-NIR spectroscopy

UV-Vis-NIR absorption spectra of hydrated and activated zeolites were recorded in a reflectance mode by using a Agilent UV-Vis-NIR Cary 5000 spectrometer equipped with a diffuse reflectance attachment with integrating sphere coated by  $\text{BaSO}_4$ . Prior to each measurement, baseline spectrum was collected by using Teflon as reference sample. Spectra were collected between 50000 to 4000  $\text{cm}^{-1}$  with a data interval of 10  $\text{cm}^{-1}$  and at a rate of 6000  $\text{cm}^{-1}/\text{min}$ . For UV-Vis-NIR measurements on activated zeolites about 0.4 grams of each samples were introduced into an “home-made” quartz cell able to work in flux conditions and allowing *in situ* experiments, high temperature treatments and gas dosages. Prior to measurements performed at room temperature, the samples were activated at 400°C for 2 hr in dry  $\text{O}_2/\text{He}$  v/v 50% flow (10 mL/min).

### 5.3.3 EPR spectroscopy

EPR spectra of hydrated and activated zeolites were collected with an X-band Bruker EMX EPR spectrometer with a Gunn diode microwave source in the field interval 2200-4000 Gauss. The fine powder samples (18-20 mg) were placed in  $\varnothing$  5 mm quartz EPR tubes fitted with  $\varnothing$  3 mm quartz tube inserts. Background spectra were collected on empty tubes and were subtracted from all reported spectra. The hydrated spectra were collected on calcined samples that had been left with full access to the atmosphere for at least 2 days after calcination. The samples were activated in a flow (10 mL/min) of dry (passed through  $\text{P}_2\text{O}_5$ )  $\text{O}_2/\text{He}$  v/v 50 % under temperature ramp from RT to 390°C (approx. 1.5 h) through the inner capillary and left at 390°C for 2 hours. The EPR spectrum of the activated sample was performed after fast cooling to RT under the same gas flow. Spectra were collected with microwave power 6.3 mW, modulation frequency 100 kHz, modulation amplitude 8 G, frequency 9.58 GHz and averaged over 10 sweeps. Tube and tube position in the cavity was kept constant. After measurement the samples were kept in the tubes and after some days with access to air the sample was measured again. The background-corrected spectra were integrated twice to compare the relative intensity. The spectra were simulated using the program WEPR95 by Neese<sup>140</sup> as a randomly oriented powder; hyperfine coupling to  $^{63/65}\text{Cu}$  was treated as a perturbation; the lineshape was Lorentzian for all simulated spectra. Quantification experiments (not shown) was performed relative to known copper(II) sulphate solid solutions in potassium sulphate. The results were very similar to the data reported in for example.<sup>24</sup>

## 6. Conclusions

High performance of small pore Cu-SSZ-13 zeolite as an NH<sub>3</sub>-SCR catalyst has encouraged fundamental studies on this material in order to explain its higher catalytic activity<sup>13,33</sup> and durability<sup>12,27</sup> in comparison with medium and large pore zeolites such as Cu-ZSM-5 or Cu-β. In the present study Cu-SSZ-13 has been well characterized by means of *in situ* FTIR, UV-Vis-NIR and EPR spectroscopies and compared with Cu-ZSM-5 and Cu-β with similar Si/Al and Cu/Al ratios and prepared following the same ion exchange procedure. As it is well known that Cu<sup>2+</sup> ions exchanged into zeolites give rise easily to Cu<sup>+</sup> species upon *vacuum* activation at temperature higher than 673 K (“self reduction” procedure),<sup>59,86</sup> the effect of this activation was compared with an O<sub>2</sub> oxidative treatment, typical of NH<sub>3</sub>-SCR process.

All the samples were studied by IR spectroscopy following the evolution of spectra upon increasing coverages of N<sub>2</sub>, CO and NO, used as probes. Each probe was used for a specific purpose, and in particular:

- N<sub>2</sub> probe revealed the presence of at least two families of Cu<sup>+</sup> sites in Cu-SSZ-13, and small amount of Al<sup>3+</sup> species (Lewis sites).
- CO probe was able to form multiple adducts showing the presence of: (i) highly unsaturated and isolated Cu<sup>+</sup> ions able to form mono-, di- and tri-carbonyls; (ii) Cu<sup>+</sup> species also in O<sub>2</sub> activated samples; (iii) monovalent [Cu–OH]<sup>+</sup> species in O<sub>2</sub> activated Cu-SSZ-13, testified by the formation of the Cu–OH⋯CO adducts (band at 2207 cm<sup>-1</sup>); (iv) changes in the acidity strength of Brønsted acid sites between the samples activated in *vacuum* and those activated in O<sub>2</sub>.
- NO underlined the high affinity towards copper species. In particular it monitored: (i) ready formation of mono- and di-nitrosyls complexes with Cu<sup>+</sup> ions; (ii) heterogeneity of the local environment of Cu<sup>2+</sup> species detected in O<sub>2</sub> activated samples (especially in case of Cu-SSZ-13) upon formation of mono-nitrosyls; (iii) presence of [Cu–OH]<sup>+</sup> in O<sub>2</sub> activated samples testified by the formation of corresponding mono-nitrosyls (band at 1890 cm<sup>-1</sup>).
- Highly informative has also been the parallel investigation of the ν(O–H) stretching region where we observed the band at 3657 cm<sup>-1</sup> ascribed to Cu–OH adducts, that undergoes progressive perturbation upon formation of Cu–OH⋯CO or Cu–OH⋯NO adducts.

O<sub>2</sub> activation treatment strongly affects the optical properties of Cu exchanged zeolites. Cu-SSZ-13 is found to be characterized by Cu<sup>2+</sup> sites located in a variety of environments but, absence of a band around 22700 cm<sup>-1</sup> excludes the presence of mono(μ-oxo)dicopper [Cu–O–Cu]<sup>2+</sup> dimers. The presence of well-resolved and intense signals in the d-d range of the visual spectrum is unique to activated Cu-SSZ-13 and results in a distinctive dark blue color. These bands persist even after

interaction with NO and NH<sub>3</sub> but disappears after exposure to H<sub>2</sub>O. The line at 22700 cm<sup>-1</sup> in O<sub>2</sub> activated Cu-ZSM-5 and Cu-β disappears after being subjected to any of these molecules.

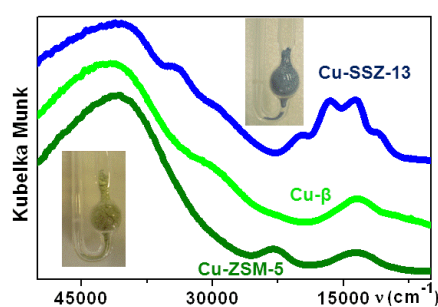
In the hydrated samples all copper is EPR active. A significant fraction of the copper species has restrained rotational freedom even in the hydrated state and both isotropic and anisotropic spectral features are visible. After dehydration water molecules bound to copper is lost and interactions with the framework results in only anisotropic copper being observed. The O<sub>2</sub> activated samples have very similar EPR spectra for all the zeolites investigated and no EPR signals due to low symmetry species or dimers are visible. The intensity of the EPR signal in the activated state, however, is much lower for Cu-SSZ-13 and Cu-ZSM-5 compared to Cu-β. Summarizing, we have identified an activation and measurement protocol sensible to the differences in the local Cu coordination symmetry and we have identified the spectroscopic fingerprint of a dark blue Cu<sup>2+</sup> species in Cu-SSZ-13 that persists even at high temperatures and after exposure to SCR conditions.

## Aknowledgments

Guan Zhang, previously Technical University of Denmark, is acknowledged for performing the EPR quantification reference curve and preliminary EPR Cu zeolite measurements. FG would like to thank Sara Morandi and Floriana Vindigni for help in building the *in situ* UV-Vis-NIR measurements set-up. SM would like to thank the Danish Research Council, Technology and Production for financial support.

## Table of contents entry

O<sub>2</sub>-activated Cu-SSZ-13 zeolite exhibits peculiar d-d quadruplet that is persistent during NH<sub>3</sub>-SCR catalytic conditions



## References

- 1 S. Roy, M. S. Hegde and G. Madras, *Appl. Ener.*, 2009, **86**, 2283.
- 2 R. Keiski, H. Raisanen, M. Harkonen, T. Maunula and P. Niemisto, *DeNO(x) reactions in lean exhaust gas conditions over metal substrated zeolite catalysts*, in: *Environmental Catalysis: For a Better World and Life*; G. Centi, S. Perathoner, C. Cristiani and P. Forzatti, Ed.; Italian Chem. Soc.: Rome, **1995**, p. 57.
- 3 P. Grange and V. I. Parvulescu, *Chem. Rev.*, 2011, **111**, 3155.
- 4 S. Brandenberger, O. Krocher, A. Tissler and R. Althoff, *Catal. Rev.*, 2008, **50**, 492.
- 5 S. Sato, Y. Yoshihiro, H. Yahiro, N. Mizuno and M. Iwamoto, *Appl. Catal.*, 1991, **70**, L1.
- 6 M. Iwamoto, *Stud. Surf. Sci. Catal.*, 1991, **60**, 327.

- 7 H. Yahiro and M. Iwamoto, *Appl. Catal. A-Gen.*, 2001, **222**, 163.
- 8 C. Lamberti, S. Bordiga, M. Salvalaggio, G. Spoto, A. Zecchina, F. Geobaldo, G. Vlaic and M. Bellatreccia, *J. Phys. Chem. B*, 1997, **101**, 344.
- 9 Y. H. Zhang, I. J. Drake and A. T. Bell, *Chem. Mater.*, 2006, **18**, 2347.
- 10 V. I. Parvulescu, P. Grange and B. Delmon, *Catal. Today*, 1998, **46**, 233.
- 11 N. Wilken, K. Wijayanti, K. Kamasamudram, N. W. Currier, R. Vedaiyan, A. Yezerets and L. Olsson, *Appl. Catal. B-Environ.*, 2012, **111**, 58.
- 12 J. H. Kwak, D. Tran, S. D. Burton, J. Szanyi, J. H. Lee and C. H. F. Peden, *J. Catal.*, 2012, **287**, 203.
- 13 J. H. Kwak, R. G. Tonkyn, D. H. Kim, J. Szanyi and C. H. F. Peden, *J. Catal.*, 2010, **275**, 187.
- 14 D. W. Fickel, E. D'Addio, J. A. Lauterbach and R. F. Lobo, *Appl. Catal. B-Environ.*, 2011, **102**, 441.
- 15 I. Bull, W. M. Xue, P. Burk, R. S. Boorse, W. M. Jaglowski, G. S. Koermer, A. Moini, J. A. Patchett, J. C. Dettling and M. T. Caudle, **2008**, U.S. Patent 7601662 B2.
- 16 S. I. Zones, **1985**, U.S. Patent US4544538 A.
- 17 A. Zecchina, S. Bordiga, J. G. Vitillo, G. Ricchiardi, C. Lamberti, G. Spoto, M. Bjorgen and K. P. Lillerud, *J. Am. Chem. Soc.*, 2005, **127**, 6361.
- 18 S. Bordiga, L. Regli, D. Cocina, C. Lamberti, M. Bjorgen and K. P. Lillerud, *J. Phys. Chem. B*, 2005, **109**, 2779.
- 19 S. Bordiga, L. Regli, C. Lamberti, A. Zecchina, M. Jorgen and K. P. Lillerud, *J. Phys. Chem. B*, 2005, **109**, 7724.
- 20 L. Regli, A. Zecchina, J. G. Vitillo, D. Cocina, G. Spoto, C. Lamberti, K. P. Lillerud, U. Olsbye and S. Bordiga, *Phys. Chem. Chem. Phys.*, 2005, **7**, 3197.
- 21 J. H. Kwak, D. Tran, J. Szanyi, C. H. F. Peden and J. H. Lee, *Catal. Lett.*, 2012, **142**, 295.
- 22 J. H. Kwak, H. Y. Zhu, J. H. Lee, C. H. F. Peden and J. Szanyi, *Chem. Comm.*, 2012, **48**, 4758.
- 23 J. Szanyi, J. H. Kwak, H. Zhu and C. H. F. Peden, *Phys. Chem. Chem. Phys.*, 2013, **15**, 2368.
- 24 F. Gao, E. D. Walter, E. M. Karp, J. Luo, R. G. Tonkyn, J. H. Kwak, J. Szanyi and C. H. F. Peden, *J. Catal.*, 2013, **300**, 20.
- 25 H. Zhu, J. H. Kwak, C. H. F. Peden and J. Szanyi, *Catal. Today*, 2013, **205**, 16.
- 26 L. M. Ren, L. F. Zhu, C. G. Yang, Y. M. Chen, Q. Sun, H. Y. Zhang, C. J. Li, F. Nawaz, X. J. Meng and F. S. Xiao, *Chem. Commun.*, 2011, **47**, 9789.
- 27 D. W. Fickel, J. M. Fedeyko and R. F. Lobo, *J. Phys. Chem. C*, 2010, **114**, 1633.
- 28 U. Deka, A. Juhin, E. A. Eilertsen, H. Emerich, M. A. Green, S. T. Korhonen, B. M. Weckhuysen and A. M. Beale, *J. Phys. Chem. C*, 2012, **116**, 4809.
- 29 U. Deka, I. Lezcano-Gonzalez, S. J. Warrender, A. L. Picone, P. A. Wright, B. M. Weckhuysen and A. M. Beale, *Micr. Mesop. Mater.*, 2013, **166**, 144.
- 30 U. Deka, I. Lezcano-Gonzalez, B. M. Weckhuysen and A. M. Beale, *ACS Catal.*, 2013, **3**, 413.
- 31 J. S. McEwen, T. Anggara, W. F. Schneider, V. F. Kispersky, J. T. Miller, W. N. Delgass and F. H. Ribeiro, *Catal. Today*, 2012, **184**, 129.
- 32 V. F. Kispersky, A. J. Kropf, F. H. Ribeiro and J. T. Miller, *Phys. Chem. Chem. Phys.*, 2012, **14**, 2229.
- 33 L. Ma, Y. Cheng, G. Cavataio, R. W. McCabe, L. Fu and J. Li, *Chem. Eng. J.*, 2013, **225**, 323.
- 34 Q. Ye, L. F. Wang and R. T. Yang, *Appl. Catal. A-Gen.*, 2012, **427**, 24.
- 35 R. Martinez-Franco, M. Moliner, C. Franch, A. Kustov and A. Corma, *Appl. Catal. B-Environ.*, 2012, **127**, 273.
- 36 T. Beutel, J. Sárkány, G. D. Lei, J. Y. Yan and W. M. H. Sachtler, *J. Phys. Chem.*, 1996, **100**, 845.
- 37 H. I. n. Praliaud, S. Mikhailenko, Z. Chajar and M. Primet, *Appl. Catal. B-Environ.*, 1998, **16**, 359.
- 38 K. Mathisen, M. Stockenhuber and D. G. Nicholson, *Phys. Chem. Chem. Phys.*, 2009, **11**, 5476.
- 39 T. Yumura, M. Takeuchi, H. Kobayashi and Y. Kuroda, *Inorg. Chem.*, 2008, **48**, 508.
- 40 P. J. Smeets, J. S. Woertink, B. F. Sels, E. I. Solomon and R. A. Schoonheydt, *Inorg. Chem.*, 2010, **49**, 3573.
- 41 K. Pierloot, A. Delabie, M. H. Groothaert and R. A. Schoonheydt, *Phys. Chem. Chem. Phys.*, 2001, **3**, 2174.
- 42 O. H. Han, C.-S. Kim and S. B. Hong, *Angew. Chem.-Int. Edit.*, 2002, **41**, 469.
- 43 S. Sklenak, J. Dedecek, C. Li, B. Wichterlova, V. Gabova, M. Sierka and J. Sauer, *Phys. Chem. Chem. Phys.*, 2009, **11**, 1237.
- 44 J. Dedecek, Z. Sobalik and B. Wichterlova, *Catal. Rev.*, 2012, **54**, 135.
- 45 S. Bordiga, C. Lamberti, F. Geobaldo, A. Zecchina, G. Turnes Palomino and C. Otero Aréan, *Langmuir*, 1995, **11**, 527.
- 46 A. Zecchina, S. Bordiga, C. Lamberti, G. Spoto, L. Carnelli and C. Otero Aréan, *J. Phys. Chem.*, 1994, **98**, 9577.
- 47 C. Lamberti, G. T. Palomino, S. Bordiga, G. Berlier, F. D'Acapito and A. Zecchina, *Angew. Chem.-Int. Edit.*, 2000, **39**, 2138.
- 48 C. Lamberti, S. Bordiga, F. Bonino, C. Prestipino, G. Berlier, L. Capello, F. D'Acapito, F. Xamena and A. Zecchina, *Phys. Chem. Chem. Phys.*, 2003, **5**, 4502.
- 49 V. Bolis, A. Barbaglia, S. Bordiga, C. Lamberti and A. Zecchina, *J. Phys. Chem. B*, 2004, **108**, 9970.
- 50 G. Spoto, E. Gribov, S. Bordiga, C. Lamberti, G. Ricchiardi, D. Scarano and A. Zecchina, *Chem. Comm.*, 2004, **23**, 2768.
- 51 Z. Li, K. C. Xie and R. C. T. Slade, *Appl. Catal. A-Gen.*, 2001, **209**, 107.
- 52 Y. Kuroda, K. Yagi, N. Horiguchi, Y. Yoshikawa, R. Kumashiro and M. Nagao, *Phys. Chem. Chem. Phys.*, 2003, **5**, 3318.

- 53 Y. H. Zhang, I. J. Drake, D. N. Briggs and A. T. Bell, *J. Catal.*, 2006, **244**, 219.
- 54 I. J. Drake, Y. H. Zhang, D. Briggs, B. Lim, T. Chau and A. T. Bell, *J. Phys. Chem. B*, 2006, **110**, 11654.
- 55 S. Bordiga, E. Groppo, G. Agostini, J. A. van Bokhoven and C. Lamberti, *Chem. Rev.*, 2013, **113**, 1736.
- 56 J. Vallyon and W. K. Hall, *J. Phys. Chem.*, 1993, **97**, 7054.
- 57 J. O. Petunchi, G. Marcelin and W. K. Hall, *J. Phys. Chem.*, 1992, **96**, 9967.
- 58 J. Sárkány, J. d'Itri and W. H. Sachtler, *Catal. Lett.*, 1992, **16**, 241.
- 59 G. T. Palomino, P. Fisticaro, S. Bordiga, A. Zecchina, E. Giamello and C. Lamberti, *J. Phys. Chem. B*, 2000, **104**, 4064.
- 60 F. X. Llabrés i Xamena, P. Fisticaro, G. Berlier, A. Zecchina, G. T. Palomino, C. Prestipino, S. Bordiga, E. Giamello and C. Lamberti, *J. Phys. Chem. B*, 2003, **107**, 7036.
- 61 B. R. Goodman, K. C. Hass, W. F. Schneider and J. B. Adams, *Catal. Lett.*, 2000, **68**, 85.
- 62 S. C. Larsen, A. Aylor, A. T. Bell and J. A. Reimer, *J. Phys. Chem.*, 1994, **98**, 11533.
- 63 G. D. Lei, B. J. Adelman, J. Sárkány and W. M. H. Sachtler, *Appl. Catal. B-Environ.*, 1995, **5**, 245.
- 64 P. Da Costa, B. Moden, G. D. Meitzner, D. K. Lee and E. Iglesia, *Phys. Chem. Chem. Phys.*, 2002, **4**, 4590.
- 65 H. J. Jang, W. K. Hall and J. L. d'Itri, *J. Phys. Chem.*, 1996, **100**, 9416.
- 66 G. T. Palomino, S. Bordiga, A. Zecchina, G. L. Marra and C. Lamberti, *J. Phys. Chem. B*, 2000, **104**, 8641.
- 67 S. T. Korhonen, D. W. Fickel, R. F. Lobo, B. M. Weckhuysen and A. M. Beale, *Chem. Comm.*, 2011, **47**, 800.
- 68 J. Dedecek, B. Wichterlova and P. Kubat, *Micr. Mesop. Mater.*, 1999, **32**, 63.
- 69 P. Vanelderden, J. Vancauwenbergh, B. F. Sels and R. A. Schoonheydt, *Coord. Chem. Rev.*, 2013, **257**, 483.
- 70 M. H. Groothaert, P. J. Smeets, B. F. Sels, P. A. Jacobs and R. A. Schoonheydt, *J. Am. Chem. Soc.*, 2005, **127**, 1394.
- 71 K. I. Hadjiivanov and G. N. Vayssilov, *Adv. Catal.*, 2002, **47**, 307.
- 72 A. Zecchina and C. O. Arean, *Chem. Soc. Rev.*, 1996, **25**, 187.
- 73 A. Zecchina, D. Scarano, S. Bordiga, G. Spoto and C. Lamberti, *Adv. Catal.*, 2001, **46**, 265.
- 74 C. Lamberti, E. Groppo, G. Spoto, S. Bordiga and A. Zecchina, *Adv. Catal.*, 2007, **51**, 1.
- 75 C. Lamberti, A. Zecchina, E. Groppo and S. Bordiga, *Chem. Soc. Rev.*, 2010, **39**, 4951.
- 76 A. Vimont, F. Thibault-Starzyk and M. Daturi, *Chem. Soc. Rev.*, 2010, **39**, 4928.
- 77 Y. Kuroda, Y. Yoshikawa, S. Konno, H. Hamano, H. Maeda, R. Kumashiro and M. Nagao, *J. Phys. Chem.*, 1995, **99**, 10621.
- 78 F. Geobaldo, C. Lamberti, G. Ricchiardi, S. Bordiga, A. Zecchina, G. T. Palomino and C. O. Arean, *J. Phys. Chem.*, 1995, **99**, 11167.
- 79 S. Bordiga, C. Pazé, G. Berlier, D. Scarano, G. Spoto, A. Zecchina and C. Lamberti, *Catal. Today*, 2001, **70**, 91.
- 80 D. D. Saperstein and A. J. Rein, *J. Phys. Chem.*, 1977, **81**, 2134.
- 81 G. L. Marra, A. N. Fitch, A. Zecchina, G. Ricchiardi, M. Salvalaggio, S. Bordiga and C. Lamberti, *J. Phys. Chem. B*, 1997, **101**, 10653.
- 82 A. Zecchina, S. Bordiga, M. Salvalaggio, G. Spoto, D. Scarano and C. Lamberti, *J. Catal.*, 1998, **173**, 540.
- 83 C. Lamberti, S. Bordiga, A. Zecchina, M. Salvalaggio, F. Geobaldo and C. O. Arean, *J. Chem. Soc.-Faraday Trans.*, 1998, **94**, 1519.
- 84 A. Zecchina, S. Bordiga, G. T. Palomino, D. Scarano, C. Lamberti and M. Salvalaggio, *J. Phys. Chem. B*, 1999, **103**, 3833.
- 85 G. T. Palomino, E. Giamello, P. Fisticaro, S. Bordiga, C. Lamberti and A. Zecchina, *Stud. Surf. Sci. Catal.*, 2000, **130**, 2915.
- 86 F. Xamena, P. Fisticaro, G. Berlier, A. Zecchina, G. T. Palomino, C. Prestipino, S. Bordiga, E. Giamello and C. Lamberti, *J. Phys. Chem. B*, 2003, **107**, 7036.
- 87 C. Prestipino, L. Regli, J. G. Vitillo, F. Bonino, A. Damin, C. Lamberti, A. Zecchina, P. L. Solari, K. O. Kongshaug and S. Bordiga, *Chem. Mater.*, 2006, **18**, 1337.
- 88 C. Lamberti, S. Bordiga, F. Geobaldo, A. Zecchina and C. Otero Aréan, *J. Chem. Phys.*, 1995, **103**, 3158.
- 89 S. Bordiga, I. Roggero, P. Ugliengo, A. Zecchina, V. Bolis, G. Artioli, R. Buzzoni, G. Marra, F. Rivetti, G. Spano and C. Lamberti, *J. Chem. Soc., Dalton Trans.*, 2000, 3921.
- 90 S. Bordiga, P. Ugliengo, A. Damin, C. Lamberti, G. Spoto, A. Zecchina, G. Spano, R. Buzzoni, L. Dalloro and F. Rivetti, *Top. Catal.*, 2001, **15**, 43.
- 91 S. H. Strauss, *J. Chem. Soc.-Dalton Trans.*, 2000, 1.
- 92 A. J. Lupinetti, S. H. Strauss and G. Frenking, *Prog. Inorg. Chem.*, 2001, **49**, 1.
- 93 V. Bolis, S. Maggiorini, L. Meda, F. D'Acapito, G. T. Palomino, S. Bordiga and C. Lamberti, *J. Chem. Phys.*, 2000, **113**, 9248.
- 94 Y. Kuroda, R. Kumashiro, T. Yoshimoto and M. Nagao, *Phys. Chem. Chem. Phys.*, 1999, **1**, 649.
- 95 Y. Kuroda, Y. Yoshikawa, R. Kumashiro and M. Nagao, *J. Phys. Chem. B*, 1997, **101**, 6497.
- 96 R. Bulanek, H. Drobna, P. Nachtigall, M. Rubes and O. Bludsky, *Phys. Chem. Chem. Phys.*, 2006, **8**, 5535.
- 97 G. Spoto, A. Zecchina, S. Bordiga, G. Ricchiardi, G. Martra, G. Leofanti and G. Petrini, *Appl. Catal. B-Environ.*, 1994, **3**, 151.
- 98 C. Prestipino, L. Capello, F. D'Acapito and C. Lamberti, *Phys. Chem. Chem. Phys.*, 2005, **7**, 1743.
- 99 A. Zecchina, S. Bordiga, G. Spoto, D. Scarano, G. Petrini, G. Leofanti, M. Padovan and C. O. Arean, *J. Chem. Soc.-Faraday Trans.*, 1992, **88**, 2959.

- 100 S. Bordiga, D. Scarano, G. Spoto, A. Zecchina, C. Lamberti and C. O. Arean, *Vib. Spectrosc.*, 1993, **5**, 69.
- 101 A. Zecchina, S. Bordiga, G. Spoto, L. Marchese, G. Petrini, G. Leofanti and M. Padovan, *J. Phys. Chem.*, 1992, **96**, 4991.
- 102 S. Bordiga, E. Escalona Platero, C. Otero Areán, C. Lamberti and A. Zecchina, *J. Catal.*, 1992, **137**, 179.
- 103 C. Lamberti, C. Morterra, S. Bordiga, G. Cerrato and D. Scarano, *Vib. Spectrosc.*, 1993, **4**, 273.
- 104 D. Scarano, S. Bordiga, C. Lamberti, G. Spoto, G. Ricchiardi, A. Zecchina and C. O. Arean, *Surf. Sci.*, 1998, **411**, 272.
- 105 K. I. Hadjiivanov, M. M. Kantcheva and D. G. Klissurski, *J. Chem. Soc., Faraday. Trans.*, 1996, **92**, 4595.
- 106 K. Gora-Marek, A. E. Palomares, A. Glanowska, K. Sadowska and J. Datka, *Micr. Mesop. Mater.*, 2012, **162**, 175.
- 107 T. T. H. Dang, H.-L. Zubowa, U. Bentrup, M. Richter and A. Martin, *Micr. Mesop. Mater.*, 2009, **123**, 209.
- 108 R. Bulanek, K. Frolich, P. Cicmanec, D. Nachtigallova, A. Pulido and P. Nachtigall, *J. Phys. Chem. C*, 2011, **115**, 13312.
- 109 G. T. Palomino, S. Bordiga, C. Lamberti, A. Zecchina and C. O. Arean, *Stud. Surf. Sci. Catal.*, 2002, **142**, 199.
- 110 C. Prestipino, G. Berlier, F. Xamena, G. Spoto, S. Bordiga, A. Zecchina, G. T. Palomino, T. Yamamoto and C. Lamberti, *Chem. Phys. Lett.*, 2002, **363**, 389.
- 111 G. Leofanti, A. Marsella, B. Cremaschi, M. Garilli, A. Zecchina, G. Spoto, S. Bordiga, P. Fisticaro, G. Berlier, C. Prestipino, G. Casali and C. Lamberti, *J. Catal.*, 2001, **202**, 279.
- 112 C. Lamberti, G. Spoto, D. Scarano, C. Pazé, M. Salvalaggio, S. Bordiga, A. Zecchina, G. T. Palomino and F. Dacapito, *Chem. Phys. Lett.*, 1997, **269**, 500.
- 113 J. Dedecek, Z. Sobalik, Z. Tvaruzkova, D. Kaucky and B. Wichterlova, *J. Phys. Chem.*, 1995, **99**, 16327.
- 114 A. Corma, V. Fornés and E. Palomares, *Appl. Catal. B-Environ.*, 1997, **11**, 233.
- 115 A. A. Davydov and A. A. Budneva, *React. Kinet. Catal. Lett.*, 1983, **25**, 121.
- 116 R. A. Schoonheydt, *J. Phys. Chem. Solids*, 1989, **50**, 523.
- 117 P. J. Smeets, M. H. Groothaert and R. A. Schoonheydt, *Catal. Today*, 2005, **110**, 303.
- 118 M. H. Groothaert, K. Lievens, H. Leeman, B. M. Weckhuysen and R. A. Schoonheydt, *J. Catal.*, 2003, **220**, 500.
- 119 G. Herzberg, *Molecular spectra and molecular structure. Vol. 2: Infrared and Raman spectra of polyatomic molecules*; Van Nostrand, Reinhold: New York, **1945**; Vol. 1, p.
- 120 F. Bonino, A. Damin, G. Ricchiardi, M. Ricci, G. Spanò, R. D'Aloisio, A. Zecchina, C. Lamberti, C. Prestipino and S. Bordiga, *J. Phys. Chem. B*, 2004, **108**, 3573.
- 121 H. A. Jahn and E. Teller, *Proc. R. Soc. A-Math. Phys. Sci.*, 1937, **161**, 220.
- 122 A. B. P. Lever, *Inorganic Electronic Spectroscopy (II ed)*; Elsevier: Amsterdam, **1984**, p. 557
- 123 J. Dedecek and B. Wichterlova, *J. Phys. Chem. B*, 1997, **101**, 10233.
- 124 C. K. Jørgensen, *The Nephelauxetic Series*, in: *Progress in Inorganic Chemistry*; F. A. Cotton, Ed.; John Wiley & Sons: Hoboken, NJ, USA, **2007**; Vol. 4 Ch. 2.
- 125 M. H. Groothaert, K. Pierloot, A. Delabie and R. A. Schoonheydt, *Phys. Chem. Chem. Phys.*, 2003, **5**, 2135.
- 126 A. Delabie, K. Pierloot, M. H. Groothaert, R. A. Schoonheydt and L. G. Vanquickenborne, *Eur. J. Inorg. Chem.*, 2002, 515.
- 127 M. H. Groothaert, K. Lievens, J. A. van Bokhoven, A. A. Battiston, B. M. Weckhuysen, K. Pierloot and R. A. Schoonheydt, *Chem. Phys. Chem.*, 2003, **4**, 626.
- 128 J. S. Woertink, P. J. Smeets, M. H. Groothaert, M. A. Vance, B. F. Sels, R. A. Schoonheydt and E. I. Solomon, *P. Natl. Acad. Sci. USA.*, 2009, **106**, 18908.
- 129 M. K. Neylon, C. L. Marshall and A. J. Kropf, *J. Am. Chem. Soc.*, 2002, **124**, 5457.
- 130 E. A. Pidko, E. J. M. Hensen and R. A. van Santen, *Proc. R. Soc. A-Math. Phys. Eng. Sci.*, 2012, **468**, 2070.
- 131 M. H. Groothaert, J. A. van Bokhoven, A. A. Battiston, B. M. Weckhuysen and R. A. Schoonheydt, *J. Am. Chem. Soc.*, 2003, **125**, 7629.
- 132 Y. Teraoka, C. Tai, H. Ogawa, H. Furukawa and S. Kagawa, *Appl. Catal. A-Gen.*, 2000, **200**, 167.
- 133 K. D. Karlin, J. C. Hayes, Y. Gultneh, R. W. Cruse, J. W. McKown, J. P. Hutchinson and J. Zubieta, *J. Am. Chem. Soc.*, 1984, **106**, 2121.
- 134 C. Eicken, F. Zippel, K. Buldt-Karentzopoulos and B. Krebs, *FEBS Lett.*, 1998, **436**, 293.
- 135 M. LoJacono, G. Fierro, R. Dragone, X. B. Feng, J. d'Itri and W. K. Hall, *J. Phys. Chem. B*, 1997, **101**, 1979.
- 136 C. Pazé, S. Bordiga, C. Lamberti, M. Salvalaggio, A. Zecchina and G. Bellussi, *J. Phys. Chem. B*, 1997, **101**, 4740.
- 137 G. Busca, L. Lietti, G. Ramis and F. Berti, *Appl. Catal. B-Environ.*, 1998, **18**, 1.
- 138 E. A. Eilertsen, B. Arstad, S. Svelle and K. P. Lillerud, *Micr. Mesop. Mater.*, 2012, **153**, 94.
- 139 M. A. Díaz-Cabañas, P. A. Barrett and M. A. Camblor, *Chem. Comm.*, 1998, **17**, 1881.
- 140 F. Neese, W. G. Zumft, W. E. Antholine and P. M. H. Kroneck, *J. Am. Chem. Soc.*, 1996, **118**, 8692.